Global Change Biology (2014), doi: 10.1111/gcb.12474

Climate-driven uncertainties in modeling terrestrial gross primary production: a site level to global-scale analysis

RAHUL BARMAN[1], ATUL K. JAIN[1] and MIAOLING LIANG[1,2]
[1]*Department of Atmospheric Sciences, University of Illinois at Urbana-Champaign, Urbana, IL, USA*

Abstract

We used a land surface model to quantify the causes and extents of biases in terrestrial gross primary production (GPP) due to the use of meteorological reanalysis datasets. We first calibrated the model using meteorology and eddy covariance data from 25 flux tower sites ranging from the tropics to the northern high latitudes and subsequently repeated the site simulations using two reanalysis datasets: NCEP/NCAR and CRUNCEP. The results show that at most sites, the reanalysis-driven GPP bias was significantly positive with respect to the observed meteorology-driven simulations. Notably, the absolute GPP bias was highest at the tropical evergreen tree sites, averaging up to ca. 0.45 kg C m^{-2} yr^{-1} across sites (ca. 15% of site level GPP). At the northern mid-/high-latitude broadleaf deciduous and the needleleaf evergreen tree sites, the corresponding annual GPP biases were up to 20%. For the nontree sites, average annual biases of up to ca. 20–30% were simulated within savanna, grassland, and shrubland vegetation types. At the tree sites, the biases in short-wave radiation and humidity strongly influenced the GPP biases, while the nontree sites were more affected by biases in factors controlling water stress (precipitation, humidity, and air temperature). In this study, we also discuss the influence of seasonal patterns of meteorological biases on GPP. Finally, using model simulations for the global land surface, we discuss the potential impacts of site-level reanalysis-driven biases on the global estimates of GPP. In a broader context, our results can have important consequences on other terrestrial ecosystem fluxes (e.g., net primary production, net ecosystem production, energy/water fluxes) and reservoirs (e.g., soil carbon stocks). In a complementary study (Barman *et al.*, 2013), we extend the present analysis for latent and sensible heat fluxes, thus consistently integrating the analysis of climate-driven uncertainties in carbon, energy, and water fluxes using a single modeling framework.

Keywords: gross primary production (GPP), Integrated Science Assessment Model (ISAM), land surface model, uncertainty

Received 7 May 2013; revised version received 5 September 2013 and accepted 8 September 2013

Introduction

The response of the terrestrial vegetation to climate is currently being investigated using both measurements and models. In conjunction with data-driven methods that provide valuable insights into biospheric responses to environmental changes (Law *et al.*, 2002; Beer *et al.*, 2010; Yi *et al.*, 2010; Jung *et al.*, 2011), land surface models (LSMs) are being used for further hypothesis testing (Sellers *et al.*, 1996a,b). LSMs are also especially important – for coupling to climate and earth system models to determine future changes (Denman *et al.*, 2007; Meehl *et al.*, 2007). However, substantial uncertainties remain in current model estimates of terrestrial carbon, energy, and water fluxes, and it is becoming increasingly necessary to quantify and reduce these uncertainties (Ahlström *et al.*, 2012; Wang & Dickinson, 2012).

One important uncertainty in the models arises from inaccuracies in input datasets itself, such as from meteorological forcings (i.e., climate). While photosynthetic assimilation in LSMs are governed based on mechanistic processes and parameterizations (Farquhar *et al.*, 1980; Ball, 1987; Collatz *et al.*, 1991, 1992; Dai *et al.*, 2004; Bonan *et al.*, 2011), the climatic/environmental controls determine the specific response and seasonality of ecosystem productivity (Churkina & Running, 1998; Law *et al.*, 2002; Nemani *et al.*, 2003; Beer *et al.*, 2010). For example, climate influences GPP through changes in solar radiation, precipitation, atmospheric temperature, and humidity (controls vapor pressure deficit) that determine the supply of light, water, and nutrient availability to plant cells. The response of GPP to warming is usually positive at low temperatures and reduces at higher temperatures, and generally increasing with photosynthetically active radiation, and decreasing with increases in vapor pressure deficit [e.g., see Fig. 2 of (Bonan *et al.*, 2011). On a longer timescale, climatic regimes also often determine the

[2] Present address: Civil and Environmental Engineering, Princeton University, Princeton, NJ, USA

Correspondence: Rahul Barman, tel. + 217 372 7134, fax + 217 372 1752, e-mail: account1.rahul@gmail.com;
Atul K. Jain, tel. + 217 333 2128, fax + 217 372 1752, e-mail: jain1@illinois.edu

photosynthetic pathway adopted by plant species (Still *et al.*, 2003). Indeed, the strength of meteorological drivers in influencing the terrestrial GPP has been documented previous studies. For example, a study over Europe (Jung *et al.*, 2007) using several terrestrial biosphere models showed that different meteorological reanalysis datasets produced comparable changes in GPP with that due to different models. At a global scale, Zhao *et al.* (2006) showed that MODIS-derived GPP ranged from ca. 101–125 GtC yr^{-1} (where GtC is gigatonne of carbon = 10^{15} g C) based on the choice of three reanalysis datasets. In LSMs with coupled biogeochemistry, these uncertainties in GPP are most likely to produce significant differences in subsequent carbon fluxes (e.g., net primary production (NPP), net ecosystem exchange (NEE), and litter fall), and in soil carbon reservoirs. In addition, given such documented uncertainties in GPP based on meteorological inputs (at regional to global scales), corresponding impacts on LSM-derived energy and water fluxes from vegetation also warrant careful study.

To systematically quantify the modeling uncertainties based on reanalysis data, a key question is: what are the uncertainties in the aforementioned fluxes after calibrating a LSM using ground-based observational data, such as from FLUXNET (Baldocchi *et al.*, 2001). Ecosystem-level measurements of above-canopy carbon, energy, and water fluxes, along with ancillary meteorological measurements are currently available at numerous FLUXNET sites (Baldocchi, 2008). To reliably use LSMs, the benefits of using such data for model calibration havepreviously been established (Friend *et al.*, 2007; Stöckli *et al.*, 2008; Williams *et al.*, 2009; Blyth *et al.*, 2010). In this context, consistently calibrating a LSM requires the use of observed site meteorology (model input) in tandem with eddy covariance data (model output for evaluation) (e.g., Stöckli *et al.*, 2008). However, for subsequent regional/global applications, the biases in meteorology fields in reanalysis datasets (Fekete *et al.*, 2004; Zhao *et al.*, 2006) are most likely to result in biased modeled fluxes.

Here, we investigate such biases in canopy fluxes from reanalysis datasets using one particular LSM – the Integrated Science Assessment Model (ISAM). The current ISAM combines the existing biogeochemical components of the model (Yang *et al.*, 2009; Jain *et al.*, 2009, 2013) with detailed biogeophysical schemes selectively adapted from several other LSMs [details in this paper; (Barman *et al.*, 2013; El-Masri *et al.*, 2013; Song *et al.*, 2013). The original goal of this integration was to extend the capability of ISAM for use in an earth system model (Barman *et al.*, 2011). A previous iteration of this model has been used in model-data intercomparison studies elsewhere (Huntzinger *et al.*, 2012; Richardson *et al.*, 2012; Schaefer *et al.*, 2012; Kauwe *et al.*, 2013). Here, we further improved the model based on FLUXNET data and used it to analyze the climate-driven biases in modeled GPP, latent heat (*LE*), and sensible heat (*H*) fluxes. We subdivided the entire analysis into two complementary studies; in the current part, we focus on GPP and present the impacts on *LE* and *H* in Barman *et al.* (2013).

Our specific objectives are as follows: (i) to present the calibration of key vegetation parameters influencing GPP, derived from model optimization at 25 FLUXNET sites; (ii) to analyze the climate-driven uncertainties in GPP directly at the site-level using two reanalysis datasets as inputs: CRUNCEP and NCEP/NCAR (references in Methods); (iii) to determine the dominant meteorological controls causing the model biases; and (iv) to discuss the corresponding impacts on global-scale modeling of GPP. Differing from previous studies based on FLUXNET data using statistical and/or diagnostic techniques (Law *et al.*, 2002; Beer *et al.*, 2010; Yi *et al.*, 2010; Jung *et al.*, 2011), our use of a LSM framework enables us to investigate the causes of these biases due to both environmental (abiotic) and plant functional/physiological (biotic) controls. Additionally, the site-level analysis adopted here allows us to consistently compare the modeled GPP biases with the driver reanalysis biases. Finally, comparable regional/global studies have focused on GPP uncertainties (Zhao *et al.*, 2006; Jung *et al.*, 2007); and the integrated analysis of uncertainties in GPP, energy/water fluxes using the same model framework – such as presented in our studies [the current study, and Barman *et al.* (2013)] has not yet been documented in literature.

Materials and methods

GPP and Carbon cycle components in ISAM

ISAM simulates carbon, energy, and water fluxes at half-hourly to hourly time steps. In the following sections, we briefly summarize the photosynthesis-related schemes and parameters in ISAM. Further details of carbon cycle processes in ISAM, including the representation of energy/water components are also available in other studies (Barman *et al.*, 2013; El-Masri *et al.*, 2013; Song *et al.*, 2013).

Photosynthesis in the model is based on a coupled 'leaf temperature – photosynthesis – stomatal conductance' scheme (Dai *et al.*, 2004). This utilizes leaf-level photosynthesis for the C_3 (Farquhar *et al.*, 1980; Collatz *et al.*, 1991) and the C_4 (Collatz *et al.*, 1992) enzyme-kinetic pathways. The stomatal conductance implementation is a variant of the Ball–Berry model (Ball, 1987; Collatz *et al.*, 1991). Leaf-level photosynthesis and stomatal conductance are scaled to the canopy level separately for sun and shaded leaves, using sun/shade canopy Leaf Area Index (LAI) fractions and scaling parameters to represent extinction of nitrogen and light through the

vertical canopy (Dai *et al*., 2004). We revised the 'two-stream' scheme of Dai *et al.* (2004) by implementing the treatment of diffuse radiation from Bonan *et al.* (2011); this reduces biases in shaded leaf photosynthesis. A day-length correction factor on V_{cmax} (maximum carboxylation rate) was also included (Bonan *et al*., 2011). Formulations of soil moisture availability in ISAM adapted from Oleson *et al.* (2008) and further modified based on El Maayar *et al.* (2009). LAI in ISAM is prescribed; however, for the herbaceous biomes, we additionally constrain the phenology to reduce biases in leaf onset/fall period (El-Masri *et al*., 2013). In the prognostic C-N configuration, GPP in ISAM is modified through the feedback of N-availability and is obtained by dynamically comparing plant N-demand and supply (El-Masri *et al*., 2013). In the diagnostic C-N configuration, we directly prescribe N-limited V_{cmax} (i.e., $V_{c\max 25}^{opt} f(N)$) (Kattge *et al*., 2009).

Data

FLUXNET data. We used eddy covariance data and ancillary meteorology from 25 sites from the FLUXNET network (Table 1, Fig. S1). The geographic range of the chosen sites span across North and South America (Table 1), varying in latitudes from approximately 22°S–71°N. The North American sites used here are a subset of the North American Carbon Program (NACP) site synthesis (Schwalm *et al*., 2010a; Schaefer *et al*., 2012), while the South American sites are a part of the Large-Scale Biosphere-Atmosphere Experiment in Amazonia (LBA) model intercomparison project (El-Masri *et al*., 2013). In ISAM (the LSM used in this study), functionally similar vegetation types in the global land surface are grouped into a finite number of plant functional types (PFTs). To optimize the model performance for global applications, we used strategic sampling by picking sites representative of major ecoclimatological types in the global land surface. Our chosen sites encompass the following PFTs used in the model: tropical broadleaf evergreen tree (Trop.BET) and broadleaf deciduous tree (Trop.BDT), temperate broadleaf deciduous tree (Temp.BDT), needleleaf evergreen tree (NET), savanna, grass, shrub, tundra, and pasture (Table 1). From the available number of sites in the NACP and the LBA syntheses, we selected sites that contained uninterrupted meteorological records during the study period, with low instability in the partitioning algorithm of NEE to GPP, and with reasonable energy balance characteristics (also see, Barman *et al*., 2013). Because our primary goal was to investigate climate-driven uncertainties in ecosystem fluxes, we limited the current study to sites without dominant anthropogenic disturbances, such as harvesting (e.g., Sakai *et al*., 2004), clear-cutting and stand-replacing fire (e.g., Krishnan *et al*., 2009; Zha *et al*., 2009). Therefore, we also did not include any crop sites in this study (due to the presence of harvesting, rotation practices, and other crop-specific processes); detailed representation of crop-specific processes in ISAM has been documented in Song *et al.* (2013). Overall, our synthesis represents a total of 84 site-years of data measured from 1997 to 2004.

Half-hourly/hourly time-series data for consistently gap-filled meteorology (Ricciuto *et al*., 2009) and GPP were available at the chosen sites (see, supplementary text S1). At sites where the total gap exceeds 15% for the data record (see, footnote of Table 1), we used published GPP estimates based on flux tower data (rather than filling the GPP gaps ourselves). For the NACP sites, the random and partitioning uncertainties in GPP were also available in the data. We computed these uncertainties for the LBA sites based on available schemes from literature (supplementary text S1). For all sites, we first combined the half-hourly/hourly random and partitioning uncertainties in quadrature and subsequently aggregated to annual timescales (± Uncertainty in Table 1). Note that the actual annual random uncertainties are most likely to be lower than our estimates – due to compensation from positive and negative uncertainties (Richardson *et al*., 2006; Baldocchi, 2008; Lasslop *et al*., 2008). However, we did not find any statistical schemes in literature quantifying this reduction; hence, the ± Uncertainty shown in Table 1 can only be used as the maximum range in random uncertainties. Also, we did not adjust the biases in flux tower GPP arising from lack of energy balance closure; hence, GPP estimates from sites with poor energy balance may be more uncertain (Wilson *et al*., 2002). Finally, there are varying degrees of confidence intervals around the FLUXNET estimates itself; notably, while the computation of GPP and respiration provided by the FLUXNET database (used here) are carried out for uniformity, the flux partitioning provided by site principal investigators may be different than that from the database. However, this is expected to have minimal consequences for the results and implications of this study.

Forcing data and model experimental setup. We performed three off-line ISAM simulations at every flux tower site: (i) *ISAM-FLUXNET* – using the observed site-level meteorology, (ii) *ISAM-NCEP* – using the NCEP/NCAR reanalysis (Qian *et al*., 2006), and (iii) *ISAM-CRUNCEP* – using the CRUNCEP reanalysis (Viovy & Ciais, 2009; Wei *et al*., 2013). For the two latter simulations, we extracted the required site-level meteorological variables from the reanalysis datasets corresponding to the location of each flux tower (supplementary text S2). The NCEP/NCAR reanalysis has been widely used in LSM-related studies (e.g., Bonan *et al*., 2011, 2012), and in remote sensing applications (Nemani *et al*., 2003; Zhao *et al*., 2006; Zhao & Running, 2010). The CRUNCEP reanalysis is a newer product, being used in several ongoing model Intercomparison projects such as the *MsTMIP* (Multi-scale Synthesis and Terrestrial Model Intercomparison Project) (http://nacp.ornl.gov/MsTMIP.shtml), and the *TRENDY* (http://dgvm.ceh.ac.uk/; Sitch *et al*., 2008).

We first used the *ISAM-FLUXNET* simulations for model optimization. Next, utilizing the site-specific *ISAM-FLUXNET* simulations as the reference ('control'), we calculated the biases in GPP from the two reanalysis-driven simulations (*ISAM-NCEP* and *ISAM-CRUNCEP*). Here, firstly, we acknowledge that such direct comparison of flux tower meteorology with those derived from coarse resolution reanalyses has its limitations. Nonetheless, spatial coherence of biases in reanalysis has been established (e.g., Zhao *et al*., 2006), and site-scale meteorology has been used to evaluate/improve global reanalysis data (Weedon *et al*., 2011) supporting the basis of our study.

Table 1 FLUXNET sites used in this study*

Site Code	Site Name	Lon [°E]	Lat [°N]	Hgt [m]	Years (Total)	Max LAI	GPP [kg C m^{-2} yr^{-1}] ISAM**	GPP [kg C m^{-2} yr^{-1}] FLUXNET† Mean‡ ± Uncertainty§	Site/Data Reference
Tropical Broadleaf Evergreen Tree (Trop.BET)									
LBA-Km34	Manaus KM34	−60.25	−2.75	50	2002–2004 (3)	6.0	3.03	2.90 ± N.A	El-Masri *et al.* (2013)
LBA-Km67	Santarem KM67	−55.25	−3.25	63	2003–2004 (2)	5.6	2.94	3.10 ± 0.63	El-Masri *et al.* (2013)
LBA-Km83	Santarem KM83	−55.25	−3.25	64	2001–2003 (3)	5.3	2.89	2.70 ± 0.61	El-Masri *et al.* (2013)
LBA-Rja	Reserva Jaru	−62.25	−10.25	60	2000–2001 (2)	5.5	2.94	3.00 ± 0.64	El-Masri *et al.* (2013)
Tropical Deciduous Evergreen Tree (Trop.BDT)									
LBA-Ban	Bananal Island	−50.25	−10.25	40	2004–2004 (1)	5.2	2.66	2.70 ± 0.63	El-Masri *et al.* (2013)
Temperate Broadleaf Deciduous Tree (Temp.BDT)									
CA-Oas	South OldAspen	−106.25	53.25	39	1997–2004 (8)	5.0	1.01	1.07 ± 0.30	Kljun *et al.* (2007)
US-Syv	Sylvania Wilderness	−89.75	45.75	36	2002–2004 (3)	7.6	1.14	1.03 ± 0.30	Desai *et al.* (2005)
US-WCr	Willow Creek	−122.25	45.75	68	1999–2004 (6)	7.3	1.11	0.95 ± 0.30	Cook *et al.* (2004)
Needleleaf Evergreen Tree (NET)									
CA-Gro	Groundhog River	−82.25	47.75	30	2004–2004 (1)	5.0	0.88	0.98 ± 0.29	McCaughey *et al.* (2006)
CA-Obs	South OldBlackSpruce	−105.25	53.75	39	2000–2004 (5)	3.1	0.68	0.78 ± 0.26	Kljun *et al.* (2007)
CA-Ojp	South OldJackPine	−104.75	53.75	28	2000–2003 (4)	3.4	0.71	0.60 ± 0.25	Kljun *et al.* (2007)
CA-Qfo	East OldSpruce	−74.75	49.25	25	2004–2004 (1)	3.6	0.67	0.64 ± 0.25	Bergeron *et al.* (2007)
US-Me3	Metolius 2nd YoungPine	−121.75	44.25	30	2004–2004 (1)	4.1	0.82	0.88 ± 0.27	Vickers *et al.* (2009)
US-NR1	Niwot Ridge	−105.75	39.75	30	1999–2004 (6)	3.4	0.67	0.80 ± 0.27	Monson *et al.* (2002)
Savanna									
US-Ton	Tonzi Ranch	−121.25	38.25	30	2002–2004 (3)	4.3	0.85	0.92 ± 0.24	Ma *et al.* (2007)
LBA-Pdg	Reserva Pe-de-Gigante	−47.75	−21.75	21	2001–2003 (3)	3.4	1.46	1.30 ± 0.30	El-Masri *et al.* (2013)
Grass									
CA-Let	Lethbridge	−113.25	49.25	4	1999–2004 (6)	2.8	0.34	0.49 ± 0.21	Flanagan and Adkinson (2011)
US-Shd¶	Shidler Tallgrass	−96.75	36.75	4.5	1998–1999 (2)	4.5	1.71	1.72 ± 0.27	Suyker *et al.* (2003)
US-Var	Vaira Ranch	−121.25	38.25	2.5	2001–2004 (4)	4.3	0.84	0.67 ± 0.23	Ma *et al.* (2007)
CA-Mer	Mer Bleue	−75.75	45.25	3	1999–2004 (6)	6.3	0.74	0.57 ± 0.25	Roulet *et al.* (2007)
US-Los	Lost Creek	−90.25	45.75	35	2001–2004 (4)	7.1	0.69	0.78 ± 0.23	Sulman *et al.* (2009)
US-SO2	Sky Oaks Old	−116.75	33.25	6	1999–2004 (6)	2.9	0.71	0.73 ± 0.20	Luo *et al.* (2007)
Tundra									
US-Atq	Atqasuk	−157.25	70.25	4.5	2004–2004 (1)	1.5	0.16	N.A.± N.A.	–
US-Brw	Barrow	−156.75	71.25	4.5	2001–2001 (1)	1.5	0.16	0.14 ± N.A.	Eugster *et al.* (2000)
Pasture									
LBA-Fns¶	Fazenda Nossa Senhora	−62.75	−11.25	8.5	2000–2001 (2)	5.5	2.12	2.20 ± 0.29	El-Masri *et al.* (2013)

*Lon (longitude) and Lat (latitude) are corresponding to the $5^{\circ} \times 0.5^{\circ}$ land grid cell center used in the model simulations. Hgt is the approximate height of the flux measurements above the surface (also used as the reference height in the model). Max LAI is the monthly maximum LAI data at each site.
**Model simulated GPP (ISAM-FLUXNET).

†For the US and Canada (CA-) sites, half-hourly flux data are available from the North American Carbon Project (NACP) Synthesis (Schaefer *et al*., 2012); For LBA sites, flux data are available from: www.lbaeco.org/lbaeco/data.htm.
‡Sites where total missing data exceeds 15% for the years used in this study, the annual GPP budget are from published FLUXNET estimates. These sites and data references are: US-SO2 (Falge *et al*., 2002); LBA-Km34, LBA-Km67, LBA-Km83, LBA-Rja, LBA-Ban, LBA-Pdg, LBA-Fns [(El-Masri *et al*., 2013), and references cited therein); US-Syv (Desai *et al*., 2005). Note that the published GPP data may not be corresponding to the exact years used in this study; however, they typically represent the annual budget of GPP which may be sufficient for model evaluation. Sites without sufficient FLUXNET data or published GPP estimates are listed as NA, not available.
§Uncertainty calculations are using FLUXNET half-hourly/hourly data, aggregated annually to maximum uncertainty ranges. For details on schemes/methods used, please refer to supplementary textS1. Uncertainty calculations could not be computed for sites where photosynthetically active radiation (PPFD) data were not available from FLUXNET (listed as NA, not available).
¶Mixed C_3/C_4 site: US-Shd - simulated as 45% C_3/55% C_4 based on species composition from Suyker *et al.* (2003); LBA-Fns - predominantly C_4 species grasses (Andreae *et al*., 2002), and was simulated as purely C_4.

Henceforth, we do not seek to reestablish these biases; rather our goal is to relate their impacts on corresponding GPP estimates. Secondly, due to the difference in spatial resolution between the NCEP/NCAR and the CRUNCEP source datasets (ca. 2.5° × 1.9° and 0.5° × 0.5°, respectively; see supplementary text S2), different spatial interpolation schemes are also likely to contribute to the resulting GPP uncertainties/biases. However, a spatial comparison between them showed consistent and regional-scale relative differences (Fig. S2); such differences are most likely to dominate the model response over those due to different interpolation schemes.

For each simulation, we prescribed the site-specific LAI climatology based on GIMMS (provided in the *MsTMIP* driver datasets). We used soil texture (sand/clay) from site records when available, else we used data from the global International Geosphere-Biosphere Program (IGBP) Global Soil Data Task Group (2000). Soil properties in ISAM also vary with soil organic carbon concentrations, which we obtained from the 0.5°×0.5° Harmonized World Soil Database (HWSD) (FAO/IIASA/ISRIC/ISSCAS/JRC, 2012) . For model spin-up, we initialized each simulation using arbitrary initial conditions: soil/vegetation temperature of 274.15 K, soil water at field capacity, and the absence of snow and leaf dew. Because the use of a prognostic C-N model configuration (available in ISAM) requires long spin-up times [in the order of thousands of years, e.g., Koven *et al*. (2013)], we used a diagnostic C-N approach in this study whereby the effect of N-limitation on photosynthesis is calibrated into the carboxylation parameter (i.e., direct use of $V_{c\max 25}^{opt} f(N)$, see the section below for details). Consequently, we spun up each site for a total of 100 years by repeating available meteorology and atmospheric [CO_2], to obtain steady state (Fig. S3).

ISAM calibration and evaluation of GPP. Using the observed meteorological input at sites, we adjusted several PFT-specific parameters to optimize the model performance with FLUXNET eddy covariance data. For PFTs with multiple flux tower sites in Table 1, we used independent sites for model optimization and evaluation. Prior to model calibration, initial estimates of tunable PFT parameters for ISAM were generally obtained from literature (Collatz *et al*., 1991, 1992; Sellers *et al*., 1996a,b; Schenk & Jackson, 2002a,b;). Beginning with these, we used the 'trial and error' approach of parameter adjustment to concurrently optimize the GPP, latent heat, and sensible heat fluxes from ISAM with the corresponding flux tower estimates. A similar model calibration approach has also been used in previous studies using the ISAM framework (El-Masri *et al*., 2013; Song *et al*., 2013). We note that several systematic model optimization methods are currently available (e.g., Raupach *et al*., 2005; Williams *et al*., 2009); nonetheless, for the specific objectives of this study, it was sufficient to use the current approach.

The values of key photosynthetic and morphological parameters related to GPP, postmodel calibration is listed in Table 2. Additional parameters related to energy/water fluxes (e.g., stomatal conductance parameters, canopy optical properties, etc.) are described in our companion study (Barman *et al*., 2013). Following model optimization, the ISAM estimated annual mean GPP was within the 'Mean ± Uncertainty' estimates from FLUXNET (Table 1; Fig. 1). At most sites, the modeled annual mean GPP difference was ≤10–15% of the annual FLUXNET mean.

The modeled GPP was strongly dependent on the carboxylation parameter $V_{c\max 25}^{opt} f(N)$. In the calibrated model, the values of $V_{c\max 25}^{opt} f(N)$ for various PFTs (Table 2) are generally consistent with those from the TRY database (Kattge *et al*., 2009, 2011). Here, the tropical and temperate tree PFTs were exceptions, where our values are much higher: for example, for Trop.BET, Kattge *et al*. (2009): 41, ISAM: 83. However, the corresponding values used in ISAM are still within the range of other measured estimates, for example, 94 (Beerling & Quick, 1995), and species dependent values >100 (Kattge & Knorr, 2007).

For the high-latitude ecosystems (e.g., NET, tundra, etc.), we also added a low-temperature stress on rubisco-dependent assimilation following the recommendation of Schaefer *et al*. (2012). In the original CoLM and CLM models (Common Land Model and Community Land Model, respectively) based on which photosynthesis schemes are adapted in ISAM, such a low-temperature constraint was only imposed on the C_4 PFTs (Dai *et al*., 2004; Bonan *et al*., 2011). We implemented an analogous constraint on the cold region C_3 PFTs (using parameter *hlti* in Table 2), which reduced the generally positive wintertime GPP bias that were also prevalent in many NACP synthesis models (Schaefer *et al*., 2012). Subsequently, this optimization of the temperature response also allowed us to use more realistic $V_{c\max 25}^{opt} f(N)$ for cold region PFTs in the model [consistent with Kattge *et al*. (2009)].

Table 2 Key PFT-dependent parameters for ISAM calibration. Only the PFTs with available site data (from Table 1) are shown

	PFT							
Parameters*	Trop.BET	Trop.BDT	Temp.BDT	NET	Savanna	Grass	Shrub	Tundra	Pasture
$V_{cmax25}^{opt} f(N)$ [μmol/m^2/s]	83	94	81	62	70(C_3) 35†(C_4)	70(C_3) 35(C_4)	40	50	70†(C_3) 35(C_4)
ε [mol-CO_2/mol-quanta]	0.08	0.08	0.06	0.06	0.06(C_3) 0.04†(C_4)	0.06(C_3) 0.04(C_4)	0.06	0.06	0.06† (C_3) 0.04(C_4)
hhti [K]	313	311	311	308	308	308	313	303	308
hlti [K]	NR‡	NR‡	275	275	NR‡ (C_3) 281†(C_4)	275(C_3) 281(C_4)	275	275	NR‡(C_3) 281(C_4)
K_n [-]	0.5	0.5	0.5	0.5	0.5	0.5	0.5	0.5	0.5
D_{50} [cm]	80	80	21	12	50	7	50	9	7
c [-]	−1.632	−1.681	−1.835	−1.880	−1.798	−1.176	−1.909	−2.621	−1.176
D_{95} [cm]	$D_{50} \times (1/0.95 - 1)^{1/c}$								

*Description of parameters: $V_{cmax25}^{opt} f(N)$ – Nitrogen-downregulated maximum rubisco capacity at top of canopy at 25 °C per leaf area; ε – Intrinsic quantum yield; *hhti* – one-half point of high-temperature inhibition function; *hlti* – one-half point of low-temperature inhibition function; K_n – coefficient of leaf nitrogen allocation within canopy; D_{50} – 50% rooting depth; c – dimensionless root shape parameter; D_{95} – 95% rooting depth. Definition of $V_{cmax25}^{opt} f(N)$ is based on Bonan *et al.* (2011); definitions of ε, *hhti*, *hlti*, and K_n are based on Dai *et al.* (2004); definitions of D_{50}, c, and D_{95} are based on Schenk & Jackson (2002a).

†Default model value was not derived from model calibration, because of unavailability of corresponding PFT sites.

‡NR, Not required for this PFT; and only implemented for cold region C_3 PFTs.

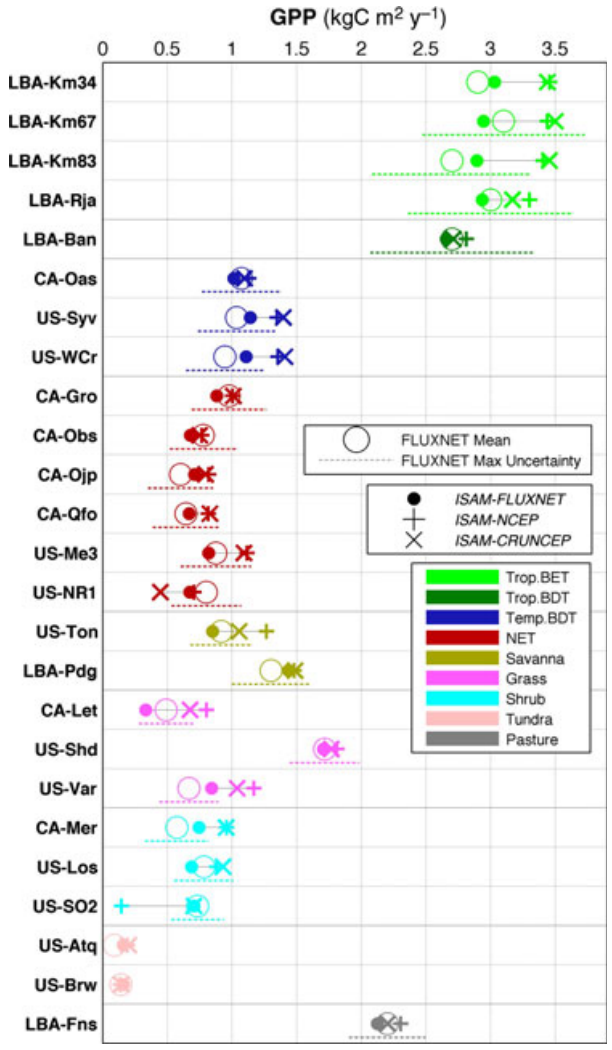

Fig. 1 Mean annual GPP at FLUXNET sites used in this study, for observational/flux data and model simulations (*ISAM-FLUXNET, ISAM-CRUNCEP, and ISAM-NCEP*). 'FLUXNET max uncertainty' denotes the ± uncertainty range from Table 1.

Another key morphological PFT control influencing GPP is the root structure. In ISAM, we used static root depth/profile for individual PFTs, based on Schenk & Jackson (2002a). However, the rooting depths of tropical trees (Trop.BET/BDT) from the aforementioned study appear to be shallow (e.g., 50% rooting depth: D_{50} = 15 cm); hence, we used a D_{50} ca. 80 cm (corresponding D_{95} ca. 4 m) for Trop.BET/BDT to improve the modeled GPP. Use of deep roots for tropical trees is consistent with other field estimates [e.g., mean root depth >3 m in Schenk & Jackson (2002b), and very deep roots of >7 m in Canadell *et al.* (1996)]. In addition, we also increased the D_{50} for savanna and shrub PFTs. To accommodate the deep roots, the maximum hydrologically active soil column depth used in ISAM was extended to 6 m [original value implemented in the model was 3.5 m based on CLM3.5 (Oleson *et al.*, 2008)].

Results

Site-level reanalysis-driven uncertainties in GPP

At each site, the model estimated mean annual GPP using the three sets of simulations are shown in Fig. 1. Using these, we computed the mean annual GPP biases in the *ISAM-NCEP* and the *ISAM-CRUNCEP* simulations with respect the *ISAM-FLUXNET* simulations. Here, we subsequently refer to these as ΔGPP (Fig. 2a). The results show that at most sites mean annual ΔGPP was positive, indicating an overestimation of GPP in the both the reanalysis-driven simulations. Only in 4 of 50 simulations (25 sites × 2 reanalysis), the corresponding ΔGPP was negative (Table S1). Overall, for the Trop.BET (4 sites), the mean annual ΔGPP was ca. 0.45 kg C m^{-2} yr^{-1} using both the reanalysis datasets, resulting in ca. 15% overestimation of *ISAM-FLUXNET* GPP (Table 3). The mean annual ΔGPP resulted in 17–19% overestimation of *ISAM-FLUXNET* GPP in the Temp.BDT (3 sites), and 11–18% for the NET (6 sites). Similarly, depending on the reanalysis meteorology used, an average annual ΔGPP of up to 20% was simulated at the savanna sites (2 sites), up to 31% at the grass sites (3 sites), and up to 21% at the shrub sites (3 sites). In the remainder of this section, we discuss the driving factors and underlying mechanisms of these biases at the site-level and/or PFT level as appropriate.

Tree/Forest (Trop.BET/BDT, Temp.BDT, NET)

Corresponding to the positive ΔGPP at the individual Trop.BET/BDT sites (Fig. 2a), the input biases in mean annual temperature (Δ*Tavg*), solar radiation (Δ*Srad*), and specific humidity (Δ*Q*) were also positive (Fig. 2b-d). From a daily climatological perspective, persistent ΔGPP were simulated for the Trop.BET throughout the year corresponding to predominantly +Δ*Tavg*, +Δ*Srad* and +Δ*Q* in both the reanalysis datasets (Fig. 3). We examined if there were any single meteorological factors dominating the GPP response/biases in these ecosystems. In this context, a simple univariate regression utilizing daily level model data from all the Trop.BET/BDT simulations produced weak R^2 for GPP vs. single

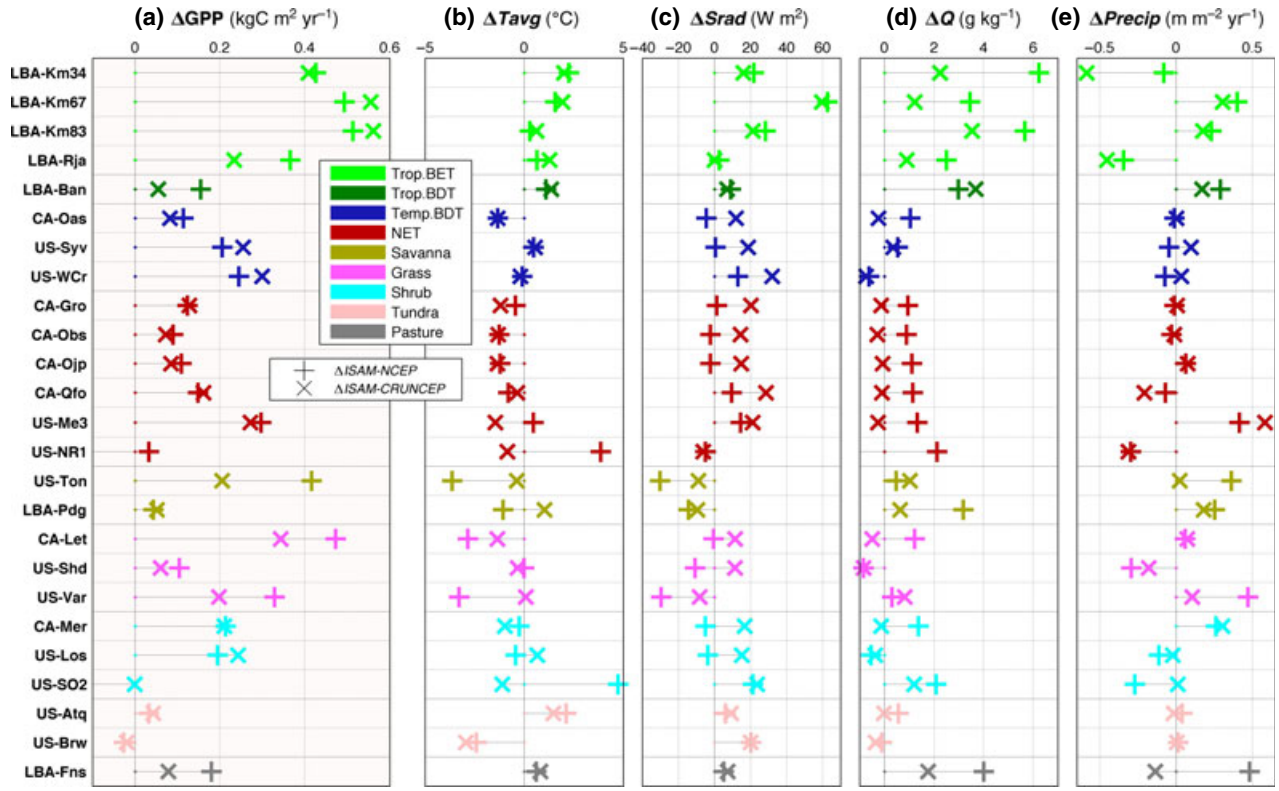

Fig. 2 (a) Site-level mean annual GPP biases (ΔGPP) in the reanalysis-driven simulations (*ISAM-CRUNCEP, ISAM-NCEP*), computed with respect to the respective *ISAM-FLUXNET* simulations. Δ*ISAM-NCEP* = *ISAM-NCEP* – *ISAM-FLUXNET*, Δ*ISAM-CRUNCEP* = *ISAM-CRUNCEP* – *ISAM-FLUXNET*. Note: negative ΔGPP at US-NR1 (using *ISAM-CRUNCEP*) and at US-SO2 (using *ISAM-NCEP*) < −0.1 kg C m^{-2} yr^{-1} were clipped from the figure axis. (b–e) Mean annual biases in input meteorology variables: (b) Δ*Tavg*, (c) Δ*Srad*, (d) Δ*Q*, and (e) Δ*Precip*.

meteorology variables (R^2: GPP vs. *Tavg*: 0.13, GPP vs. *Srad*: 0.22, GPP vs. *Q*: 0.30; see Fig. S4a), showing that no single variable dominating the GPP response.

Table 3 Site averaged annual GPP and biases, grouped by PFTs. ΔCRUNCEP = *ISAM-CRUNCEP* – *ISAM-FLUXNET*, ΔNCEP = *ISAM-NCEP* – *ISAM-FLUXNET*. The values in parenthesis are percentage differences of GPP with respect to*ISAM-FLUXNET*

		GPP [kg C m^{-2} yr^{-1}]		
PFT	Sites	*ISAM-FLUXNET*	ΔCRUNCEP	ΔNCEP
Trop.BET	4	2.95	0.44(15)	0.45(15)
Trop.BDT	1	2.66	0.05(2)	0.15(6)
Temp.BDT	3	1.09	0.21(19)	0.19(17)
NET	6	0.74	0.08(11)	0.13(18)
Savanna	2	1.14	0.13(11)	0.23(20)
Grass	3	0.96	0.20(21)	0.30(31)
Shrub	3	0.71	0.15(21)	−0.05(−7)
Tundra	2	0.16	0.01(7)	0.00(2)
Pasture	1	2.12	0.08(4)	0.18(8)

Previously, other modeling studies also showed that productivity in ecosystems is generally a result of non-linear interactions of several meteorological and environmental factors (including LAI, soil properties, and hydrology); hence, a generic dependence between GPP and a single environmental control may not be expected (e.g., Churkina & Running, 1998). Nonetheless, in the model simulations using the observed meteorology (*ISAM-FLUXNET*), there were large decreases in *daily* GPP coincident with reductions in daily S*rad* and *Tavg* at the individual Trop.BET/BDT sites (Fig. S5). Such reductions of *Srad* and *Tavg* in the FLUXNET meteorology data (most likely due to cloudy events) were not present in the reanalysis datasets. Consequently, the associated daily reductions in GPP were also absent. Aggregated annually, such reductions in daily GPP in the *ISAM-FLUXNET* simulations significantly contributed to the positive annual ΔGPP in the reanalysis-driven simulations. In addition, the mean annual Δ*Q* in the NCEP/NCAR was also consistently positive (generally true at other sites as well), which

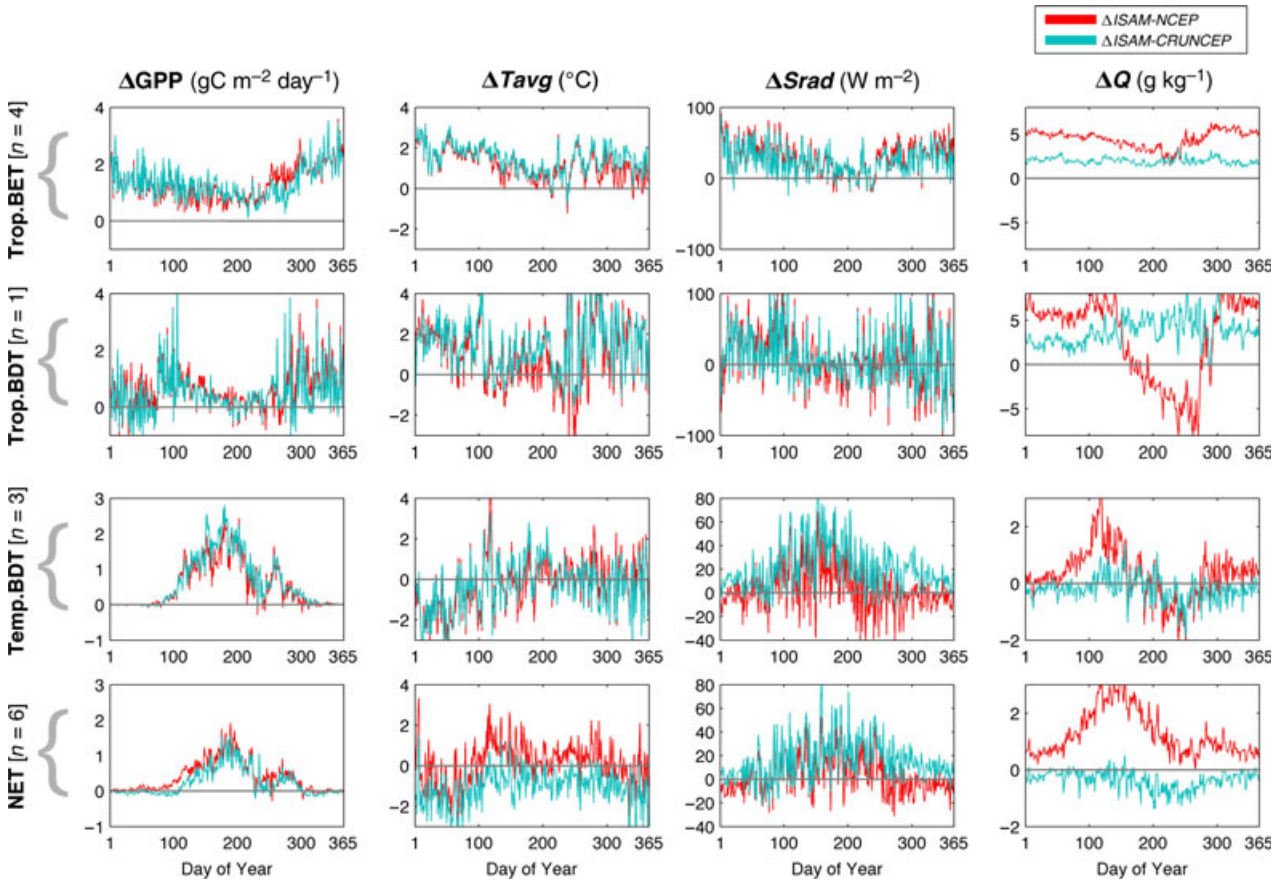

Fig. 3 Analysis for tree PFTs (Trop.BET, Trop.BDT, Temp.BDT, and NET): daily climatology of reanalysis-driven ΔGPP, Δ*Tavg*, Δ*Srad* and Δ*Q* – all averaged over the available number of sites (n) for each PFT. All the biases (Δ) were calculated with respect to the *ISAM-FLUXNET* counterpart. Each row corresponds to a PFT group (name on left corner). Each column shows a variable (name on top). For each subplot, the *x*-axis is the 'Day of year' and the *y*-axis is the respective variable.

helped to alleviate the atmospheric vapor pressure deficit (VPD), thereby further increasing the +ΔGPP.

The GPP at the Trop.BET/BDT sites did not appear to be water stressed from precipitation (during the analyzed years), as shown by the lack of root water stress at the annual scale (modeled annual mean soil water availability factor (β_t) ca. 1, Fig. 4). This was also further indicated by the lack of correlation between GPP and annual total precipitation (*Precip*) across the Trop.-BET/BDT sites (Fig. S4b). Hence, for these sites, the water availability was not a factor in controlling the GPP biases. Indeed, at two of the Trop.BET sites (LBA-Km34, LBA-Rja), where mean annual Δ*Precip* was negative in both the CRUNCEP and the NCEP/NCAR, the resulting ΔGPP were still largely positive (Fig. 2a, e). Hence, based on our analysis, the +ΔGPP for the Trop.-BET/BDT are most likely to be robust irrespective of the ± annual Δ*Precip* in the reanalysis datasets.

In contrast to the seasonally persistent ΔGPP Trop.-BET/BDT sites, the reanalysis-driven ΔGPP for the Temp.BDT (3 sites) and NET (6 sites) were confined during the growing season, with maximum positive biases during the peak of the growing season (Fig. 3). However, similar to the Trop.BET/BDT, the simulated +ΔGPP at the individual Temp.BDT and NET sites could firstly be attributed to the presence of many days with low *Srad* in the observed FLUXNET meteorology data – a major factor in the resulting +Δ*Srad* (Fig. 3). Annually, the mean +Δ*Srad* of ca. 10–30 W/m^2 were present at individual Temp.BDT and NET sites in the CRUNCEP data, and very small +Δ*Srad* in NCEP/NCAR (Fig. 2c). Nonetheless, during the growing season, the mean Δ*Srad* were significantly positive in both the reanalysis datasets, with maximum amplitudes during the peak of the growing season (Fig. 3). Overall, at the Temp.BDT and NET sites, larger +Δ*Q* in the NCEP/NCAR favored increased +ΔGPP in *ISAM-NCEP*, while a larger +Δ*Srad* in the CRUNCEP increased +ΔGPP in *ISAM-CRUNCEP* by more than offsetting the impacts of slightly negative Δ*Q* (individual sites: Fig. 2; PFT averages: Fig. 3).

The Temp.BDT and NET sites were also characterized by water stress (e.g., β_t ranging from ca. 0.5–0.75 in the *ISAM-FLUXNET* simulations, see Fig. 4). Note that, the water stress in the model is dependent on *Precip* (determining total input water), *Tavg* (controlling soil freeze/thaw processes and hence availability of *liquid* water), and other factors. Hence, depending on the amount of annual *Precip* input using the reanalysis datasets, the ± Δ*Precip* may alleviate/strengthen the water stress, impacting ΔGPP in these ecosystems. This was, for example, clearly evident at the US-Me3 NET site where larger +Δ*Precip* in the reanalysis datasets favored large +ΔGPP (Fig. 2) by alleviating the water stress (Fig. 4). A strong water stress was also evident at the US-NR1 NET site using the CRUNCEP data (β_t ca. 0.37, Fig. 4), which was the only forest/tree site in our study to simulate a negative ΔGPP (-34% in comparison with *ISAM-FLUXNET*, Table S1). This was most likely driven by both the large −Δ*Precip* and −Δ*Q* at this site.

Nontree and herbaceous (Savanna, Grass, Shrub, Tundra, Pasture). As opposed to the usually consistent seasonality of ΔGPP within the forest/tree PFT sites, large differences in seasonality and magnitudes of ΔGPP were simulated across individual sites within this category (Fig. 5). These differences could be attributed to the larger North/South range of geographical location of sites within a PFT, plant physiological differences in C_3 vs. C_4 pathways, as well as on the direction (sign) of specific meteorological biases. For example, of the two contrasting savanna sites (US-Ton, LBA-Pdg), the

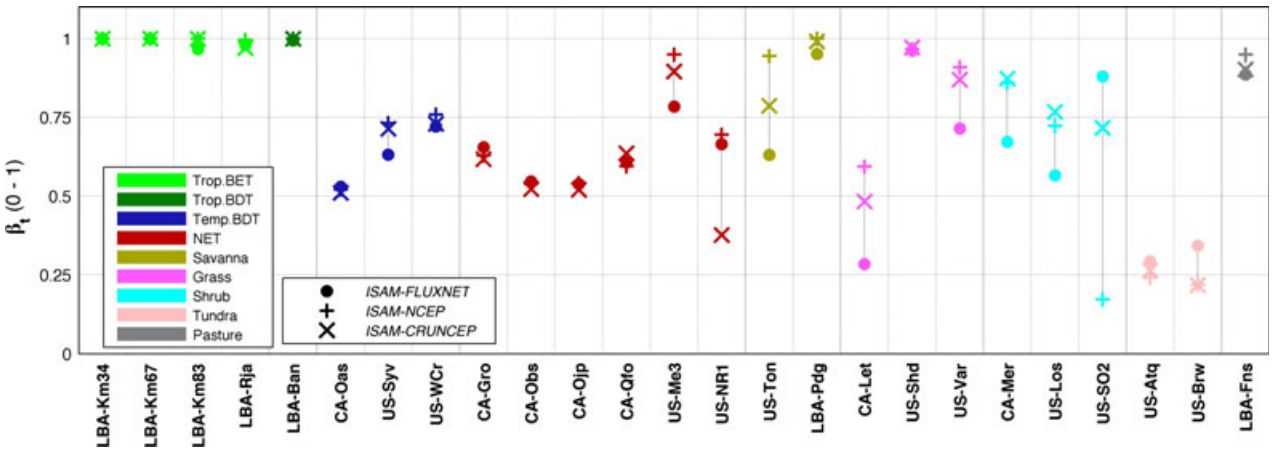

Fig. 4 Modeled annual mean soil water availability factor (β_t) at each site. A value of 1 implies no soil moisture stress on photosynthesis, while 0 implies no available water to plant roots.

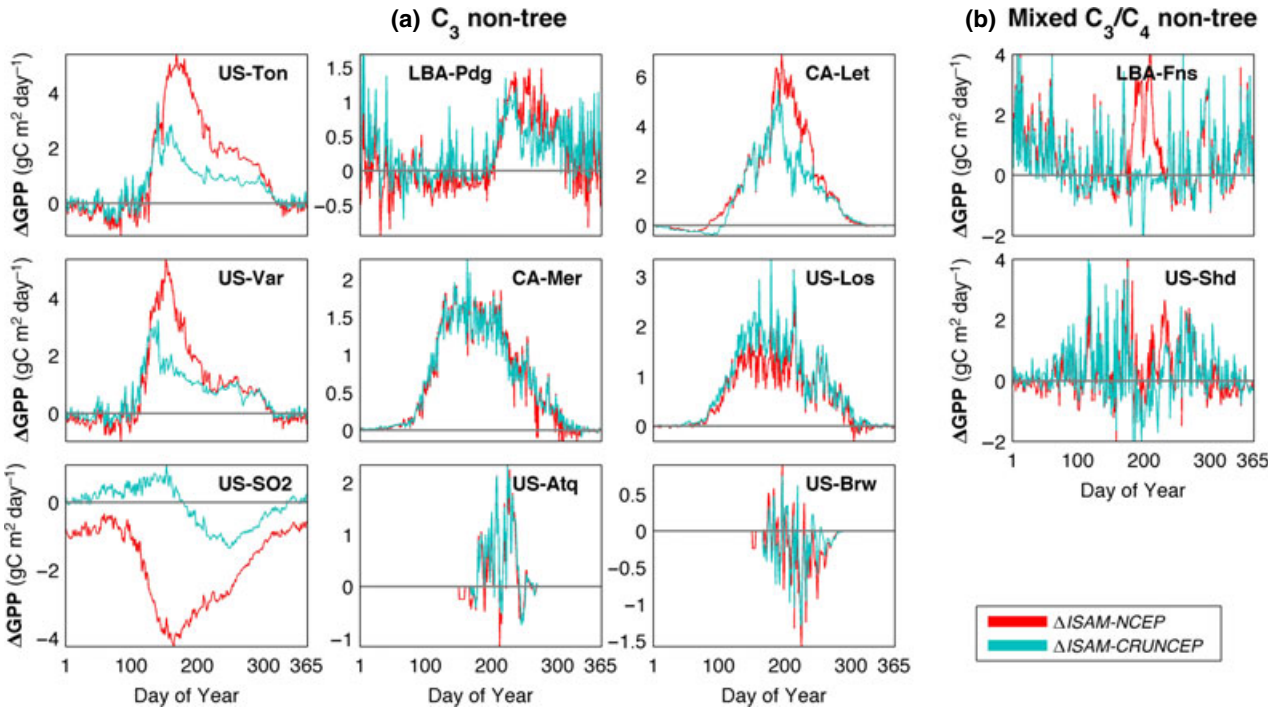

Fig. 5 Analysis for individual nontree C_3 and C_4 sites: Daily climatology of ΔGPP in reanalysis-driven simulations for the (a) nontree C_3 and (b) C_4 sites. For each subplot, the *x*-axis is the 'day of year' and the *y*-axis is ΔGPP. All the biases (Δ) were calculated with respect to the *ISAM-FLUXNET* counterpart.

mid-latitude US-Ton site simulated large +ΔGPP (0.20–0.42 kg C m^{-2} yr^{-1}, an overestimation of 24–49% in comparison with *ISAM-FLUXNET*), while the ΔGPP at the tropical LBA-Pdg site was minimal (3–4% overestimation). Large +ΔGPP also occurredat both the C_3 grass sites: CA-Let (103–142% overestimation) and US-Var (23–39% overestimation). Similarly, the ΔGPP at two of the three shrub sites (CA-Mer, US-Los) were >25% in both the reanalysis simulations. In contrast to the C_3 grass sites, the ΔGPP at the mixed C_3/C_4 sites (US-Shd: grass, LBA-Fns: pasture) were relatively smaller throughout the year in both the datasets (4–8% bias, Table S1). However, due to the limited number of C_4 sites available for our analysis, it was not clear if the relatively lower ΔGPP was a result of small meteorological biases at the analyzed sites, or if they were characteristic of C_4 physiology in general. Hence, more C_4 sites may be necessary to robustly indicate the impacts of climate-driven GPP biases for these PFTs. In general, more nontree sites will be beneficial for robustly analyzing the magnitudes of ΔGPP across the global land surface. Nonetheless, based on the available sites, several mechanisms driving the ΔGPP were evident, which are discussed as follows.

At the aforementioned C_3 savanna/grass/shrub sites where large positive ΔGPP was simulated, in all the instances, the reanalysis meteorology significantly alleviated the soil moisture stress by increasing β_t (Fig. 2). For example, β_t at US-Ton increased from ca. 0.62 in *ISAM-FLUXNET* to ca. 0.9 for *ISAM-NCEP*. At CA-Let, the corresponding increase was from 0.25 to >0.5; and at CA-Mer and US-Los, the respective β_t increased by ca. 0.25. These strongly indicate that the decrease in soil water stress in the *ISAM-NCEP* and the *ISAM-CRUNCEP* simulations was a strong factor in producing the +ΔGPP. Further analyses show that the reduction of water stress in the reanalysis-driven simulations could be associated with one or more of the following mechanisms. (i) Alleviation of high-temperature stress on carboxylation: some sites indicated a high-temperature stress on GPP, as shown by negative slope of GPP vs. *Tavg* beyond a temperature optima (e.g., US-Ton, US-Var, US-SO2 in Fig. 6). At these sites, the negative instances of daily Δ*Tavg* in the reanalysis data produced higher +ΔGPP (Fig. S6). Because higher temperatures in dry regions are also usually accompanied by higher solar radiation [e.g., see Falge *et al.* (2002)], the modeled GPP also showed a decreasing trend with increasing *Srad*. (ii) Reduction of VPD from −Δ*Tavg* and +Δ*Q*: in many of the nontree sites, the annual Δ*Tavg* was negative and Δ*Q* was positive (Fig. S6), resulting in lower atmospheric dryness. Because these PFTs are usually limited by strong water-stress, lowering of atmospheric dryness also contributed to

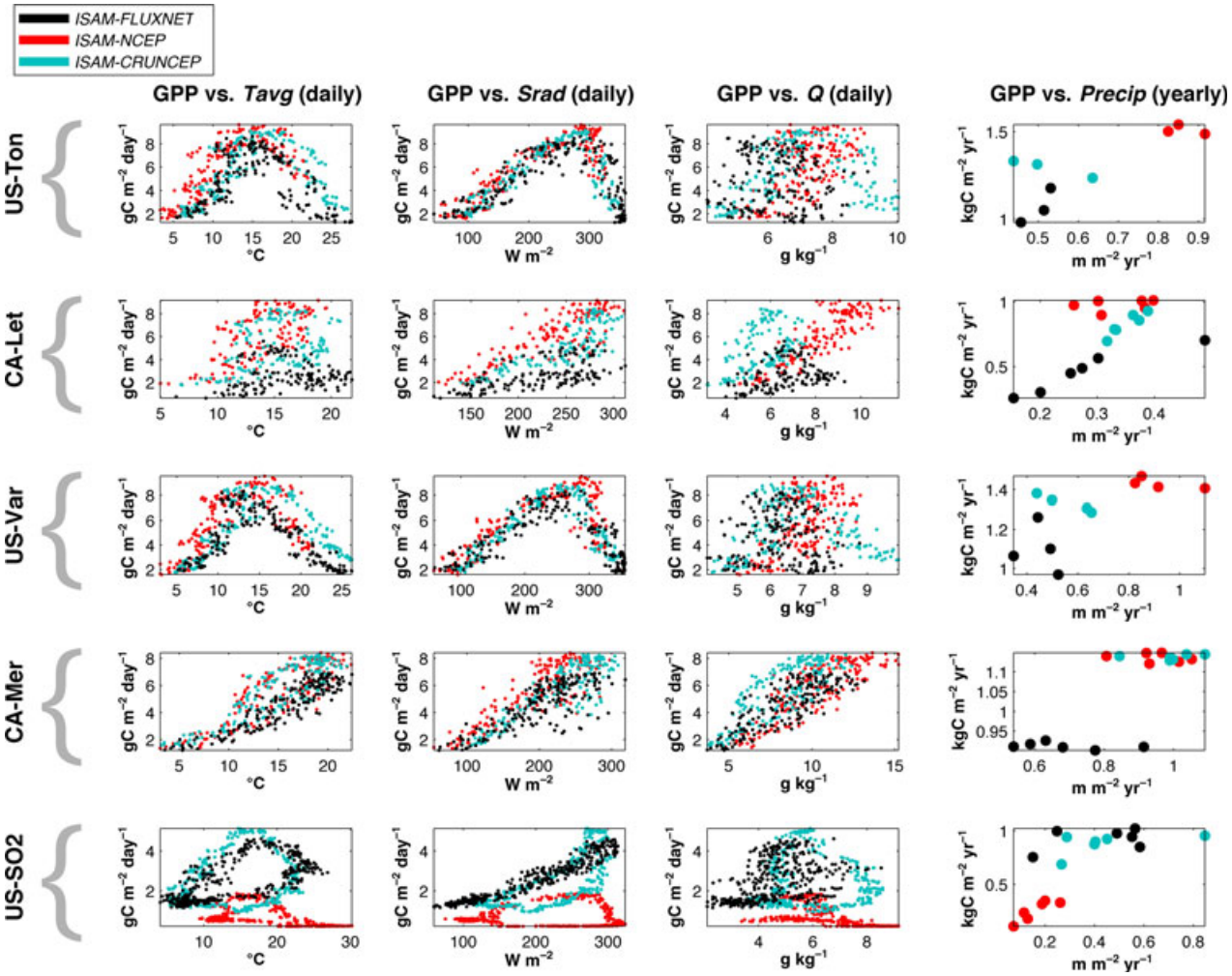

Fig. 6 Analysis for C_3 sites (only a subset of the sites are shown): daily climatology of GPP vs. *Tavg*, *Srad* and *Q*, respectively, (left group); yearly GPP vs. *Precip* (right group). Each row of subplots corresponds to an individual site (site name on left corner). For each subplot, the *x*-axis is the respective column variable (name on top) and the *y*-axis is the GPP. Note the use of daily vs. annual timescales in the individual GPP-meteorology plots. Because GPP responds to changes in *Tavg*, *Srad* and *Q* on an hourly to subdaily timescale, these respective variables were plotted using daily model output; *Precip* (which controls soil water availability) influences GPP on monthly to annual timescales, and hence, annual model output was used for the GPP vs. *Precip* plot.

the increase in GPP. (iii) Annual $+\Delta Precip$ to directly supplement the soil moisture: for example, at US-Ton, CA-Let, US-Var, CA-Mer, US-SO2 (Fig. 6). For example, at US-Ton, the $\Delta Precip$ of 0.4 m m^{-2} yr^{-1} in the NCEP/NCAR strongly contributed to the corresponding mean annual ΔGPP of 49%. Among the savanna/shrub/grass sites, only the US-SO2 shrub site simulated a very negative ΔGPP using NCEP/NCAR. At this site, the dominant drivers of the ΔGPP were the mean annual $-\Delta Precip$ (ca. −0.25 m m^{-2} yr^{-1}), as well as the mean annual $+\Delta Tavg$ (5 °C) that increased atmospheric VPD. Note that, due to the very large −ΔGPP at US-SO2 using NCEP/NCAR, the averaged ΔGPP from 3 shrub sites used in this study was negative (Table 3).

Finally, in the extreme high-latitude tundra sites (US-Atq, US-Brw), the $\Delta Tavg$ appeared to provide the dominant control over ΔGPP. At US-Brw, even in the presence of significantly positive mean annual $\Delta Srad$ in both the reanalysis datasets, the large negative $\Delta Tavg$ in both the datasets (ca. −2.5 °C, Fig. 2) resulted in negative ΔGPP (accompanied by increase in soil water stress). On the other hand, at US-Atq, the corresponding mean annual $\Delta Tavg$ and ΔGPP were both positive.

Global uncertainties in modeled GPP

As opposed to the site-level analysis, it is not possible to accurately quantify the global-extent of climate-driven GPP biases in a LSM framework due to the lack of

required global scale data (i.e., observed subdaily meteorology data at all model grid cells) to do so. Nonetheless, it may still be possible to assess the overall consistencies and differences in the reanalysis-driven GPP in a LSM by comparing with other observationally derived estimates. Here, an important caveat is that for global comparisons, other sources of uncertainty are also present, such as the land-use and land-cover change datasets (Meiyappan & Jain, 2012), the accuracy of LAI datasets (Lawrence & Chase, 2007), the presence of multiple crop types and rotation practices (i.e., human influence).Notably, although ISAM contains representation of specific crop processes such as harvest, corn-soybean rotation, etc. (Song *et al.*, 2013), in this study, we used a single PFT for global crops (though retaining the observed C_3/C_4distribution in the model; see, Fig. S7). This is because the global land cover dataset used here only contains 'generic' crops (Meiyappan & Jain, 2012), and specific crop types have not yet been implanted for the global application of the model (similar to most other LSMs). The effects of such simplifications require extensive evaluation, and here, we only focus on the meteorological aspect of the GPP biases/uncertainties.

We compared the mean annual GPP during 2000–2004 from the *ISAM*-NCEP and the *ISAM-CRUNCEP* simulations with two different sources for globally gridded GPP: (i) FLUXNET-MTE (Jung *et al.*, 2011), and (ii) MODIS (MOD17) (Zhao *et al.*, 2006; Zhao & Running, 2010) (Fig. 7). For consistency, all the GPP estimates (ISAM, FLXNET-MTE, and MODIS) were compared based on the 0.5° × 0.5° ISAM land mask, and any nonvegetated grid cells were removed from all the sources (based on the vegetation mask in Fig. S8). The resulting zonally averaged mean annual GPP estimates are shown in Fig. 8, which forms the basis for this discussion.

Globally, the *relative* GPP difference between *ISAM-NCEP* and *ISAM-CRUNCEP* was only ca. 4 GtC yr^{-1}, the *ISAM-NCEP* being slightly higher than the *ISAM-CRUNCEP* (Fig. 8a). However, because both the reanalysis-driven simulations were positively and similarly biased with respect to the site-level *ISAM-FLUXNET* simulations, the relatively small GPP differences using the two reanalysis datasets does not imply good agreement with observations at a global scale. This was evident when we compared our estimates with one of the MODIS-derived GPP estimates that used a daily

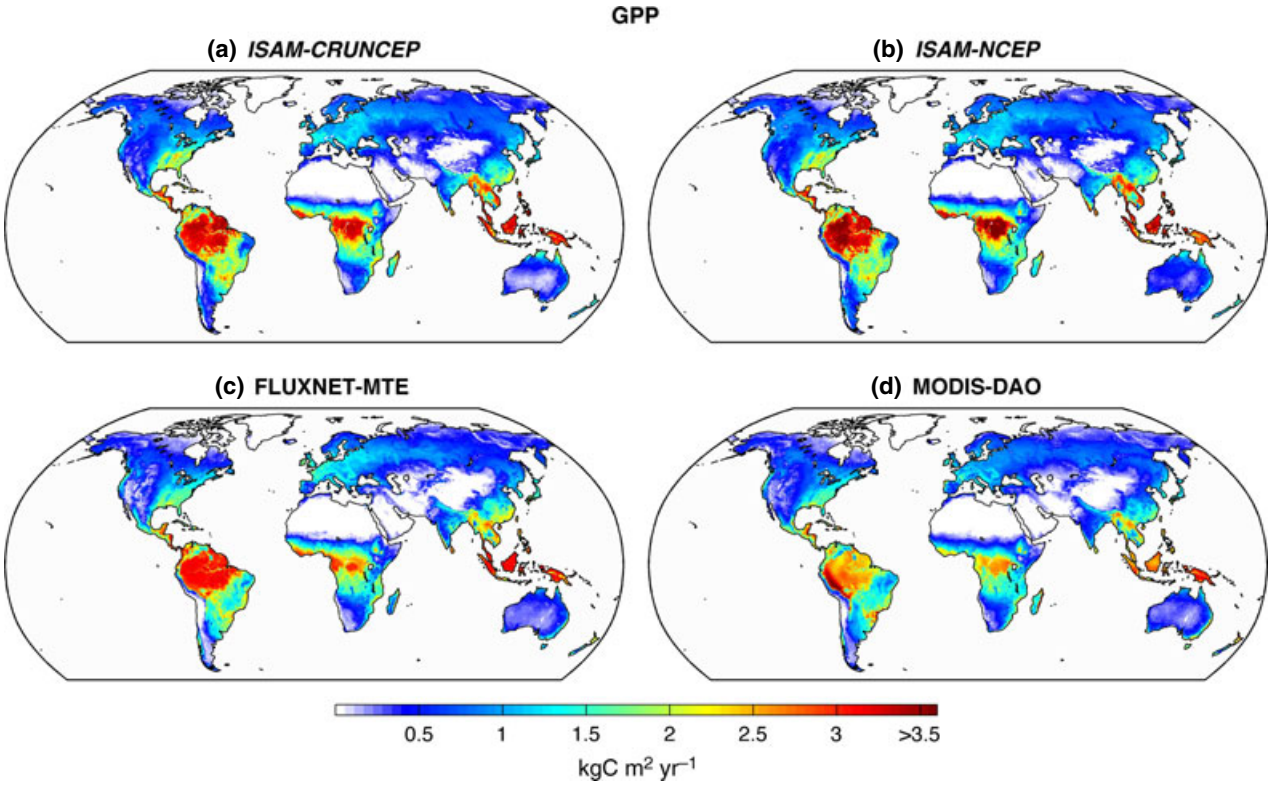

Fig. 7 Maps of mean annual estimates of GPP, for two reanalysis-driven model simulations (*ISAM-CRUNCEP* (a), *ISAM-NCEP* (b)) and observationally derived datasets [FLUXNET-MTE (c), MODIS-DAO (d)]. All the results are based on averaged output for 2000–2004 and are only for vegetated land surfaces (Fig. S8).

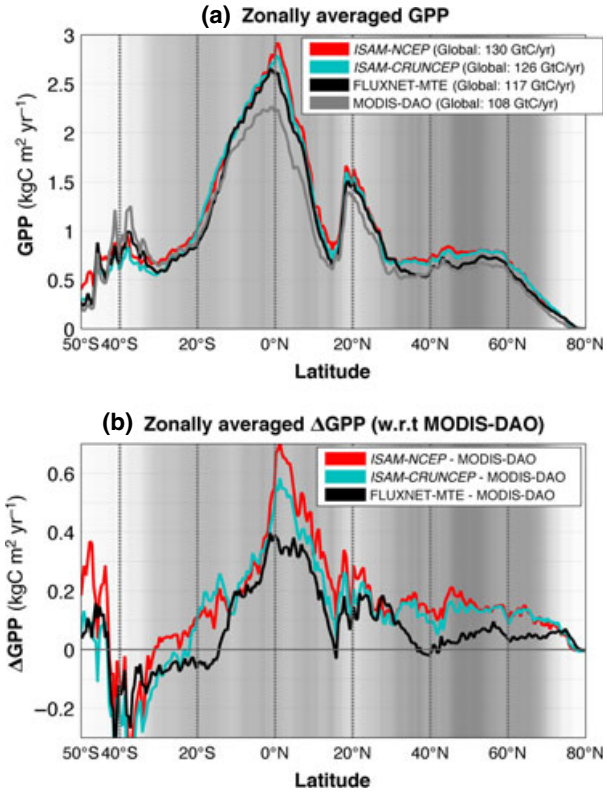

Fig. 8 (a) Zonally averaged mean annual estimates for GPP, for two reanalysis-driven model simulations (*ISAM-CRUNCEP* and *ISAM-NCEP*) and observationally derived data (FLUXNET-MTE, and MODIS-DAO). All the results are based on averaged output for 2000–2004 and are only for vegetated land surfaces (Fig. S8). The fractional land area (vegetated) at each latitude is shown as a gray scale, where darker shades represent more vegetated areas. (b) Zonally averaged GPP difference with respect to MODIS based on results from (a).

reanalysis with small meteorological biases (Zhao *et al.*, 2006) (MODIS-DAO in Fig. 8a-b). In comparison with this data, the ISAM simulations overestimated GPP across the tropical/subtropical to the northern high-latitudes, with maximum differences of ca. 0.5 kg C m^{-2} yr^{-1} at the deep tropics (also consistent with our site-level biases). Only between 20–40°S (with low-vegetation coverage), the ISAM simulations underestimated GPP relative to the MODIS-DAO-derived estimates (see, Fig. 8b). However, here, we note that the southernmost site used in our analysis (LBA-Pdg) was located at ca. 21.75°S (with all other sites being northward of ca. 11°S); hence, more Southern Hemispheric flux tower sites need to be utilized in our model calibration, to better quantify flux biases in this region. Globally, using the NCEP-NCER dataset, Zhao *et al.* (2006) also simulated a much higher GPP vs. that using the NASA-DAO meteorology (ca. 125 GtC yr^{-1} vs. 108 GtC yr^{-1}, respectively). In comparison with their study, our ISAM-derived GPP using NCEP/NCAR (ca. 130 GtC yr^{-1}) compared favorably. Here, assuming a + 10–20% bias in the reanalysis-driven global GPP using ISAM (representative of site-level GPP biases), our corresponding 'bias-corrected' GPP would reduce to ca. 105–118 GtC yr^{-1}. These 'bias-corrected' GPP from ISAM were consistent with the MODIS estimates of ca. 108 GtC yr^{-1} using the NASA-DAO meteorology.

The global GPP from FLUXNET-MTE (ca. 117 GtC yr^{-1}) was higher in comparison with MODIS-DAO (Fig. 8a, b). Still, the GPP from *ISAM-NCEP* was ca. 10% higher than that from FLUXNET-MTE. In comparison with MODIS-DAO, one likely reason for the higher tropical GPP in FLUXNET-MTE is the higher coverage of C_4 herbaceous PFTs in the tropics in the latter dataset (i.e., causing more productivity). In this study, we used the land cover distribution from Meiyappan & Jain (2012), which contains lower C_4vegetation fraction in the tropics (Fig. S7) than that used in FLUXNET-MTE [see, supplementary Fig. 6 from Beer *et al.* (2010)]. This most likely did offset the GPP differences between FLUXNET-MTE and ISAM in the tropics. Another potential reason may be due to the use of different meteorology to generate the FLUXNET-MTE product, which may be subjected to meteorological biases/differences in comparison with NASA-DAO as well as the reanalysis datasets used in our study.

Discussion

In this study, we adopted a site-level approach to investigate the reanalysis-driven GPP biases using a LSM framework and analyzed the role of biotic and environmental factors in the vegetation response. To achieve this, we first calibrated and evaluated the model for various PFTs using site-level eddy covariance and meteorology data. We subsequently applied the model at the same sites using two reanalysis meteorological datasets (the NCEP/NCAR and the CRUNCEP) to assess the extents of annual and seasonal GPP biases with respect to the FLUXNET meteorology simulations (referred to as ΔGPP). Quantification of seasonal biases in simulated GPP is especially important, as it can help to explain problems in simulating seasonal changes in NEE (Schaefer *et al.*, 2012).

Using the ISAM as the modeling tool, the results show that at most sites (and PFTs) both the NCEP/NCAR and CRUNCEP significantly overestimated the GPP, resulting in ΔGPPof up to ca. 0.45 kg C m^{-2} yr^{-1} for the tropical forest PFTs (Fig. 2). For other PFTs, even though the magnitude of the ΔGPP was smaller than those for the tropical forests, the% bias in GPP was significant: i.e., up to +10–20% for the Temp.BDT

and NET, and up to ca. +20–30% for savanna, grassland, and shrubland (Table 3). Here, one relevant question is, can we choose a preferred reanalysis dataset for model forcing between the NCEP/NCAR and the CRUNCEP? Because both the reanalysis datasets produced similarly (positive) biased GPP, one may not be preferred over the other. Nonetheless, in Barman *et al.* (2013), we show that the CRUNCEP-driven latent and sensible heat fluxes were generally in better agreement than the NCEP/NCAR counterpartswhen compared with the FLUXNET estimates. Hence, for the overall estimation of carbon, energy, and water fluxes, we recommend the use of CRUNCEP data for subsequent global applications of the ISAM.

At the Trop.BET/BDT sites, major contributions to the simulated +ΔGPP were from the +Δ*Srad* in both the reanalysis datasets. Indeed, as also shown in our further analysis (Fig. S9), in all ecosystems, the increases in +ΔGPP were majorly contributed by the sun-lit canopy, due to enhanced radiation levels at the top of the canopy. Using the observed meteorology data in the model, the Trop.BET/BDT showed strong radiation limitation on GPP during cloudy days, which was also consistent with results from site-level field experiments conducted in the Amazon forest (e.g., Graham *et al*., 2003). For the Temp.BDT/NET, the +Δ*Srad* in CRUNCEP and the +Δ*Q* in NCEP/NCAR during the growing season played key roles in producing the respective GPP biases in these PFTS. Here we also note that, even though the GPP at Temp.BDT and NET have been previously characterized as temperature-limited (e.g., Falge *et al*., 2002; Law *et al*., 2002), the annual ΔGPP were still positive at the sites with annual negative Δ*Tavg* (exception: US-NR1). This is most likely because: (i) much of the daily negative Δ*Tavg* may occur during the winter (Fig. 3 for Temp.BDT and NET) when the GPP and ΔGPP are negligible, and (ii) the overall seasonality of daily temperature is very large in the mid-/high-latitude sites (<−20 °C to >25 °C; see, Fig. 4a), and hence, a small negative annual Δ*Tavg* in the reanalysis data may not sufficiently decrease the GPP to offset the +ΔGPP from +Δ*Srad* and/or +Δ*Q*. Such a model response is also consistent with Beer *et al.* (2010), who suggested that the changes in GPP in boreal and temperate forests were robust against small variations in temperature. An implication of this result is that the annual mean ΔTavg may not be a proper indicator for the reanalysis-driven annual ΔGPP in these ecosystems.

At the C_3 savanna/grass/shrub sites, the environmental factors controlling water stress (i.e., *Tavg*, *Q*, *Precip*) dominated the resulting GPP biases. For these PFTs, the reanalysis meteorology produced notably +ΔGPP (except at the US-SO2 shrub site, which was strongly limited by annual *Precip* in the NCEP/NCAR reanalysis data). In comparison with the positive and generally significant ΔGPP at the C_3 nontree sites, the biases at the analyzed C_4 sites (savanna, grass) were relatively minimal. However, it was not clear if the low ΔGPP would be representative of other sites/regions of dominant C_4 vegetation – due to the limited number of C_4 sites available for our analysis (both for model calibration and evaluation). Finally, at the very high-latitude tundra sites, the mean annual Δ*Tavg* in both the reanalysis datasets sites controlled the sign of the ΔGPP (absolute magnitude generally small). In any case, because the total contribution from the tundra toward the global GPP is very small (1.6 GtC yr^{-1}, or <1.5% of global) (Beer *et al*., 2010), the ΔGPP from tundra may be inconsequential for global estimates.

We recognize several potential limitations in our results, arising due to existing limitations in model structure and parameters. Firstly, due to the use of prescribed LAI climatology in ISAM, it is restricting to simulate the inter-annual variability of GPP. To reduce this limitation, implementation of dynamic LAI schemes in ISAM is currently in progress. Secondly, the use of static root profiles in ISAM introduces limitations in modeling of soil water stress, and vegetation acclimation to water stress. Dynamic roots are especially important in the drier tropical and subtropical nontree ecosystems (e.g., C_3/C_4 grass, C_3/C_4 savanna, C_3/C_4 pasture, and shrubs) that have shallow root depths and where roots may vary seasonally (e.g., Arora & Boer, 2003). Besides the root profiles, the accuracy of soil moisture schemes used in the model are also important because soil water availability and water stress play significant roles in our results. Currently, there are known limitations (Zeng & Decker, 2009) of the numerical scheme used in ISAM [originally adapted from Oleson *et al.* (2008), which is used in CLM3.5]. There are other potentially important climate-driven biotic effects that are not included in this study, such as the temperature acclimation of photosynthesis (Kattge & Knorr, 2007). In the future, improvements in these and other aspects that are common to many LSMs (Schaefer *et al*., 2012) are expected to improve the modeling of carbon cycle processes in ISAM. There are also impacts from limited flux tower data availability and access. For example, only a few nontree PFT sites (i.e. fewer sites per PFT) were used in this study. As previously discussed, this imposed several limitations in our model calibration and evaluation. We particularly note the scarcity of C_4 and subtropical sites, which did limit our ability to tune multiple PFT-specific parameters for such vegetation types. From the perspective of modeling the global terrestrial carbon cycle, it is very important to properly

constrain and quantify climate-driven GPP biases in C_4 vegetation, because the C_4 vegetation covers a large expanse of the global land surface and has large contribution (>20%) to global GPP (Beer *et al*., 2010). These considerations generally indicate that more nontree sites will be beneficial for robustly calibrating carbon cycle processes in ISAM, and subsequently for analyzing the magnitudes of carbon flux biases across the global land surface. Previously, another study by Schwalm *et al.* (2010b) also suggested that larger numbers of flux tower sites are required globally to robustly analyze the drought sensitivity of vegetation types such as cropland, shrubland, and savanna and that additional flux towers are required for all vegetation types in Africa and Asia. In general, other model-data intercomparison studies have found that current ecosystem models can better simulate GPP and NEE at forest sites than at grassland sites (Schwalm *et al*., 2010a; Schaefer *et al*., 2012).

While we investigated the impacts of reanalysis data on GPP at site level, the overarching goal of such a study is ultimately to understand the consequences for global applications. Because estimates of globally gridded GPP are usually derived using meteorological reanalysis datasets, the resulting total GPP are also most likely to contain climate-driven biases within themselves. While it is not possible to exactly quantify the global total GPP biases in a LSM framework using reanalysis datasets, our site-level results suggest that these biases are expected to be of significance for the global GPP estimates. Overall, the extent of annual GPP biases using our LSM framework appear to be generally consistent with the work of Zhao *et al.* (2006) (MODIS derived GPP). In this context, we showed that assuming a range of +10–20% overall bias in our global GPP estimates (*ISAM-NCEP* ca. 130 GtC yr^{-1}, *ISAM-CRUNCEP* ca. 126 GtC yr^{-1}), the corresponding 'bias-corrected' GPP be reduced to ca. 105–118 GtC yr^{-1}. These estimates are closer to the observationally derived estimates of MODIS-DAO ca. 108 GtC yr^{-1} and FLUXNET-MTE ca. 117 GtC yr^{-1}. However, here, we should point out that beyond the similarities in global GPP estimates between this study and Zhao *et al.* (2006), the driving factors for ΔGPP may sometimes be different using our LSM-based approach. For example, because their 'light use efficiency'–based GPP model is a linear function of VPD, their GPP biases were often predominantly determined by VPD biases. Henceforth, due to the nonlinear dependence of VPD on *Tavg*, a relatively small *Tavg* bias could substantially influence the GPP bias in their analysis. In contrast, the 'Ball–Berry' scheme used in our analysis does not directly use VPD for GPP calculations; rather, the GPP is coupled directly with humidity, temperature, soil water stress, and leaf stomatal conductance. Hence, the ΔGPP in our results were not as strongly determined by Δ*Tavg*. Nonetheless, the role of Δ*Tavg* remains important in our simulations in modeling soil water availability (from freeze/thaw processes), as well as for the temperature stress on leaf carboxylation.

The sensitivity of LSM-estimated GPP to meteorology, as demonstrated in this study, highlights the importance of using standardized meteorological forcings in various LSM intercomparison projects to consistently compare the model performance. Because many projection studies using LSMs make use of earth system model (ESM) output of meteorological variables, the resulting carbon estimates should also be dependent on the accuracy of the ESM output. Similarly, the currently available globally gridded GPP 'datasets' based on FLUXNET data [e.g., Beer *et al.* (2010), Jung *et al.* (2011)] that were up-scaled using global meteorology products, should also contain a component of climate-driven biases. However, we cannot speculate on the magnitudes of GPP biases therein, as they are likely to depend on both the meteorology dataset, as well as the diagnostic method used for globally interpolating the GPP.

Finally, within the framework of a LSM, the GPP biases are also directly and indirectly coupled to corresponding biases in energy and water fluxes (Barman *et al*., 2013), with potentially important impacts on soil hydrology and energetics. Uncertainties/biases in these model processes (including their seasonal biases) should also impact other carbon fluxes such as net primary production and net ecosystem production, as well as modeled soil carbon pools. Especially in the mid- and high-latitude regions where plant respiration and soil decomposition rates are slower, the extent of GPP biases as shown in this study may be expected to significantly affect the litter fall and the soil carbon accumulation processes. In future studies, it will be important to investigate these in detail, to explain and to quantitatively reduce the current uncertainties in modeling carbon and energy/water cycle processes in LSMs.

Acknowledgements

This study was partly supported by the National Aeronautics and Space Administration (NASA) Land Cover and Land Use Change Program (No. NNX08AK75G), and U.S. Department of Energy (DOE) Office of Science (DOE-DE-SC0006706). RB was funded by the NASA Earth and Space Science Fellowship (NNX11AP85H). We thank Dr. Bassil El-Masri and Yang Song for contributing in various stages our model development. We specially thank the FLUXNET community and the P.I.s of the sites used in this study, for their continuous efforts of data collection.

References

Ahlström A, Schurgers G, Arneth A, Smith B (2012) Robustness and uncertainty in terrestrial ecosystem carbon response to CMIP5 climate change projections. *Environmental Research Letters*, **7**, 044008.

Andreae M, Artaxo P, Brandao C, Carswell F, Ciccioli P, Da Costa A, Grace J (2002) Biogeochemical cycling of carbon, water, energy, trace gases, and aerosols in amazonia: the LBA-EUSTACH experiments. *Journal of Geophysical Research: Atmospheres (1984–2012)*, **107**, LBA 331-1–LBA 33-25.

Arora VK, Boer GJ (2003) A representation of variable root distribution in dynamic vegetation models. *Earth Interactions*, **7**, 1–9.

Baldocchi D (2008) TURNER REVIEW no. 15'.breathing'of the terrestrial biosphere: lessons learned from a global network of carbon dioxide flux measurement systems. *Australian Journal of Botany*, **56**, 1–26.

Baldocchi D, Falge E, Gu L, Olson R, Hollinger D, Running S, Evans R (2001) FLUXNET: a new tool to study the temporal and spatial variability of ecosystem-scale carbon dioxide, water vapor, and energy flux densities. *Bulletin of the American Meteorological Society*, **82**, 2415–2434.

Ball J (1987) A model predicting stomatal conductance and its contribution to the control of photosynthesis under different environmental conditions. Prog Photosynthesis Res Proc Int Congress 7th, Providence. 10-15 Aug 1986. Vol 4. Kluwer, Boston. pp. 221–224.

Barman R, Hoffman FM, Lawrence DM, Song Y, Meiyappan P, Jain AK, Vertenstein M (2011) Studying uncertainties in climate-terrestrial biogeochemical feedbacks in the northern high latitudes using a flexible earth system modeling framework. AGU Fall Meeting Abstracts, 1 04.

Barman R, Jain AK, Liang M (2013) Climate-driven uncertainties in modeling terrestrial energy and water fluxes: a site-level to global scale analysis. *Global Change Biology*, doi: 10.1111/gcb.12473.

Beer C, Reichstein M, Tomelleri E, Ciais P, Jung M, Carvalhais N, Bonan GB (2010) Terrestrial gross carbon dioxide uptake: global distribution and covariation with climate. *Science*, **329**, 834–838.

Beerling D, Quick W (1995) A new technique for estimating rates of carboxylation and electron transport in leaves of C3 plants for use in dynamic global vegetation models. *Global Change Biology*, **1**, 289–294.

Bergeron O, Margolis HA, Black TA, Coursolle C, Dunn AL, Barr AG, Wofsy SC (2007) Comparison of carbon dioxide fluxes over three boreal black spruce forests in Canada. *Global Change Biology*, **13**, 89–107.

Blyth E, Clark D, Ellis R, Huntingford C, Los S, Pryor M, Sitch S (2010) A comprehensive set of benchmark tests for a land surface model of simultaneous fluxes of water and carbon at both the global and seasonal scale. *Model Dev Discuss*, **3**, 1829–1859.

Bonan GB, Lawrence PJ, Oleson KW, Levis S, Jung M, Reichstein M, Swenson SC (2011) Improving canopy processes in the community land model version 4 (CLM4) using global flux fields empirically inferred from FLUXNET data. *Journal of Geophysical Research*, **116**, G02014.

Bonan GB, Oleson KW, Fisher RA, Lasslop G, Reichstein M (2012) Reconciling leaf physiological traits and canopy flux data: Use of the TRY and FLUXNET databases in the community land model version 4. *Journal of Geophysical Research: Biogeosciences (2005–2012)*, **117**, G02026, doi: 10.1029/2011JG001913.

Canadell J, Jackson R, Ehleringer J, Mooney H, Sala O, Schulze E (1996) Maximum rooting depth of vegetation types at the global scale. *Oecologia*, **108**, 583–595.

Churkina G, Running SW (1998) Contrasting climatic controls on the estimated productivity of global terrestrial biomes. *Ecosystems*, **1**, 206–215.

Collatz GJ, Ball JT, Grivet C, Berry JA (1991) Physiological and environmental regulation of stomatal conductance, photosynthesis and transpiration: a model that includes a laminar boundary layer. *Agricultural and Forest Meteorology*, **54**, 107–136.

Collatz GJ, Ribas-Carbo M, Berry J (1992) Coupled photosynthesis-stomatal conductance model for leaves of C4 plants. *Functional Plant Biology*, **19**, 519–538.

Cook BD, Davis KJ, Wang W, Desai A, Berger BW, Teclaw RM, Yi C (2004) Carbon exchange and venting anomalies in an upland deciduous forest in northern wisconsin USA. *Agricultural and Forest Meteorology*, **126**, 271–295.

Dai Y, Dickinson RE, Wang Y (2004) A two-big-leaf model for canopy temperature, photosynthesis, and stomatal conductance. *Journal of Climate*, **17**, 2281–2299.

Denman KL, Brasseur G, Chidthaisong A, Ciais P, Cox PM, Dickinson RE, Jacob D (2007) Couplings between changes in the climate system and biogeochemistry. *Climate Change*, **2007**, 541–584.

Desai AR, Bolstad PV, Cook BD, Davis KJ, Carey EV (2005) Comparing net ecosystem exchange of carbon dioxide between an old-growth and mature forest in the upper midwest USA. *Agricultural and Forest Meteorology*, **128**, 33–55.

El Maayar M, Price DT, Chen JM (2009) Simulating daily, monthly and annual water balances in a land surface model using alternative root water uptake schemes. *Advances in Water Resources*, **32**, 1444–1459.

El-Masri B, Barman R, Meiyappan P, Song Y, Liang M, Jain AK (2013) Carbon dynamics in the amazonian basin: integration of eddy covariance and ecophysiological data with a land surface model. *Agricultural and Forest Meteorology*, **19**, 1759–1779.

Eugster W, Rouse WR, Pielke RA Sr, Mcfadden JP, Baldocchi DD, Kittel TG, Vaganov E (2000) Land–atmosphere energy exchange in arctic tundra and boreal forest: available data and feedbacks to climate. *Global Change Biology*, **6**, 84–115.

Falge E, Baldocchi D, Tenhunen J, Aubinet M, Bakwin P, Berbigier P, Davis KJ (2002) Seasonality of ecosystem respiration and gross primary production as derived from FLUXNET measurements. *Agricultural and Forest Meteorology*, **113**, 53–74.

FAO/IIASA/ISRIC/ISSCAS/JRC. (2012) *Harmonized World Soil Database (version 1.10)*, FAO, Rome, Italy and IIASA, Laxenburg, Austria.

Farquhar G, Von Caemmerer SV, Berry J (1980) A biochemical model of photosynthetic CO2 assimilation in leaves of C3 species. *Planta*, **149**, 78–90.

Fekete BM, Vörösmarty CJ, Roads JO, Willmott CJ (2004) Uncertainties in precipitation and their impacts on runoff estimates. *Journal of Climate*, **17**, 294–304.

Flanagan LB, Adkinson AC (2011) Interacting controls on productivity in a northern Great Plains grassland and implications for response to ENSO events. *Global Change Biology*, **17**, 3293–3311.

Friend AD, Arneth A, Kiang NY, Lomas M, Ogee J, Rödenbeck C, Viovy N (2007) FLUXNET and modelling the global carbon cycle. *Global Change Biology*, **13**, 610–633.

Global Soil Data Task Group. (2000) Global Gridded Surfaces of Selected Soil Characteristics (IGBP-DIS). Available at [http://www.daac.ornl.gov] from Oak Ridge National Laboratory Distributed Active Archive Center, Oak Ridge, Tennessee, USA doi: 10.3334/ORNLDAAC/569.

Graham EA, Mulkey SS, Kitajima K, Phillips NG, Wright SJ (2003) Cloud cover limits net CO2 uptake and growth of a rainforest tree during tropical rainy seasons. *Proceedings of the National Academy of Sciences*, **100**, 572–576.

Huntzinger D, Post WM, Wei Y, Michalak A, West TO, Jacobson A, Hayes D (2012) North american carbon program (NACP) regional interim synthesis: terrestrial biospheric model intercomparison. *Ecological Modelling*, **232**, 144–157.

Jain A, Yang X, Kheshgi H, McGuire AD, Post W, Kicklighter D (2009) Nitrogen attenuation of terrestrial carbon cycle response to global environmental factors. *Global Biogeochemical Cycles*, **23**, GB4028, doi: 10.1029/2009GB003519.

Jain AK, Meiyappan P, Song Y, House JI (2013) CO_2 emissions from land-use change affected more by nitrogen cycle, than by the choice of land-cover data. *Global Change Biology*, **19**, 2893–2906.

Jung M, Vetter M, Herold M, Churkina G, Reichstein M, Zaehle S, Chen Y (2007) Uncertainties of modeling gross primary productivity over europe: a systematic study on the effects of using different drivers and terrestrial biosphere models. *Global Biogeochemical Cycles*, **21**, GB4021, doi: 10.1029/2006GB002915.

Jung M, Reichstein M, Margolis HA, Cescatti A, Richardson AD, Arain MA, Chen J (2011) Global patterns of land-atmosphere fluxes of carbon dioxide, latent heat, and sensible heat derived from eddy covariance, satellite, and meteorological observations. *Journal of Geophysical Research: Biogeosciences (2005–2012)*, **116**, doi: 10.1029/2010JG001566.

Kattge J, Knorr W (2007) Temperature acclimation in a biochemical model of photosynthesis: a reanalysis of data from 36 species. *Plant, Cell & Environment*, **30**, 1176–1190.

Kattge J, Knorr W, Raddatz T, Wirth C (2009) Quantifying photosynthetic capacity and its relationship to leaf nitrogen content for global-scale terrestrial biosphere models. *Global Change Biology*, **15**, 976–991.

Kattge J, Diaz S, Lavorel S, Prentice I, Leadley P, Bönisch G, Wright I (2011) TRY–a global database of plant traits. *Global Change Biology*, **17**, 2905–2935.

Kauwe MG, Medlyn BE, Zaehle S, Walker AP, Dietze MC, Hickler T, Prentice C(2013) Forest water use and water use efficiency at elevated CO2: a model-data intercomparison at two contrasting temperate forest FACE sites. *Global Change Biology*, 1759–1779, doi: 10.1111/gcb.12164.

Kljun N, Black T, Griffis T, Barr A, Gaumont-Guay D, Morgenstern K, Nesic Z (2007) Response of net ecosystem productivity of three boreal forest stands to drought. *Ecosystems*, **10**, 1039–1055.

Koven C, Riley W, Subin Z, Tang J, Torn M, Collins W, Swenson S (2013) The effect of vertically-resolved soil biogeochemistry and alternate soil C and N models on C dynamics of CLM4. *Biogeosciences Discussions*, **10**, 7201–7256.

Krishnan P, Black TA, Jassal RS, Chen B, Nesic Z (2009) Interannual variability of the carbon balance of three different-aged Douglas-fir stands in the pacific northwest.

Journal of Geophysical Research: Biogeosciences (2005–2012), **114**, G04011, doi: 10.1029/2008JG000912.

Lasslop G, Reichstein M, Kattge J, Papale D (2008) Influences of observation errors in eddy flux data on inverse model parameter estimation. *Biogeosciences Discussions*, **5**, 751–785.

Law B, Falge E, Gu LV, Baldocchi D, Bakwin P, Berbigier P, Fuentes J (2002) Environmental controls over carbon dioxide and water vapor exchange of terrestrial vegetation. *Agricultural and Forest Meteorology*, **113**, 97–120.

Lawrence PJ, Chase TN (2007) Representing a new MODIS consistent land surface in the community land model (CLM 3.0). *Journal of Geophysical Research: Biogeosciences (2005–2012)*, **112**, G01023, doi: 10.1029/2006JG000168.

Luo H, Oechel WC, Hastings SJ, Zulueta R, Qian Y, Kwon H (2007) Mature semiarid chaparral ecosystems can be a significant sink. *Global Change Biology*, **13**, 386–396.

Ma S, Baldocchi DD, Xu L, Hehn T (2007) Inter-annual variability in carbon dioxide exchange of an oak/grass savanna and open grassland in california. *Agricultural and Forest Meteorology*, **147**, 157–171.

McCaughey J, Pejam M, Arain M, Cameron D (2006) Carbon dioxide and energy fluxes from a boreal mixedwood forest ecosystem in ontario, canada. *Agricultural and Forest Meteorology*, **140**, 79–96.

Meehl GA, Stocker TF, Collins WD *et al.* (2007) Global climate projections. In: *Climate Change 2007: The Physical Science Basis. Contribution of Working Group I to the Fourth Assessment Report of the Intergovernmental Panel on Climate Change* (eds Solomon S, Qin D, Manning M, Chen Z, Marquis M, Averyt KB, Tignor M, Miller HL). Cambridge University Press, Cambridge, UK.

Meiyappan P, Jain AK (2012) Three distinct global estimates of historical land-cover change and land-use conversions for over 200 years. *Frontiers of Earth Science*, **6**, 122–139.

Monson R, Turnipseed A, Sparks J, Harley P, Scott-Denton L, Sparks K, Huxman T (2002) Carbon sequestration in a high-elevation, subalpine forest. *Global Change Biology*, **8**, 459–478.

Nemani RR, Keeling CD, Hashimoto H, Jolly WM, Piper SC, Tucker CJ, Running SW (2003) Climate-driven increases in global terrestrial net primary production from 1982 to 1999. *Science*, **300**, 1560–1563.

Oleson K, Niu G, Yang Z, Lawrence D, Thornton P, Lawrence P, Levis S (2008) Improvements to the community land model and their impact on the hydrological cycle. *Journal of Geophysical Research: Biogeosciences (2005–2012)*, **113**, G1.

Qian T, Dai A, Trenberth KE, Oleson KW (2006) Simulation of global land surface conditions from 1948 to 2004 Part I: forcing data and evaluations. *Journal of Hydrometeorology*, **7**, 953–975.

Raupach M, Rayner P, Barrett D, DeFries R, Heimann M, Ojima D, Schmullius C (2005) Model–data synthesis in terrestrial carbon observation: methods, data requirements and data uncertainty specifications. *Global Change Biology*, **11**, 378–397.

Ricciuto D, Thornton P, Schaefer K, Cook R, Davis K (2009) How uncertainty in gapfilled meteorological input forcing at eddy covariance sites impacts modeled carbon and energy flux. AGU Fall Meeting Abstracts, 1 03.

Richardson AD, Hollinger DY, Burba GG, Davis KJ, Flanagan LB, Katul GG, Suyker AE (2006) A multi-site analysis of random error in tower-based measurements of carbon and energy fluxes. *Agricultural and Forest Meteorology*, **136**, 1–18.

Richardson AD, Anderson RS, Arain MA, Barr AG, Bohrer G, Chen G, Desai AR (2012) Terrestrial biosphere models need better representation of vegetation phenology: results from the north american carbon program site synthesis. *Global Change Biology*, **18**, 566–584.

Roulet NT, Lafleur PM, Richard PJH, Moore TR, Humphreys ER, Bubier J (2007) Contemporary carbon balance and late Holocene carbon accumulation in a northern peatland. *Global Change Biology*, **13**, 397–411.

Sakai RK, Fitzjarrald DR, Moraes OL, Staebler RM, Acevedo OC, Czikowsky MJ, Miranda V (2004) Land-use change effects on local energy, water, and carbon balances in an amazonian agricultural field. *Global Change Biology*, **10**, 895–907.

Schaefer K, Schwalm CR, Williams C *et al.* (2012) A model-data comparison of gross primary productivity: results from the north american carbon program site synthesis. *Journal of Geophysical Research: Biogeosciences (2005–2012)*, **117**, G03010, doi: 10.1029/2012JG001960.

Schenk HJ, Jackson RB (2002a) The global biogeography of roots. *Ecological Monographs*, **72**, 311–328.

Schenk HJ, Jackson RB (2002b) Rooting depths, lateral root spreads and belowground/above-ground allometries of plants in water-limited ecosystems. *Journal of Ecology*, **90**, 480–494.

Schwalm CR, Williams CA, Schaefer K, Anderson R, Arain MA, Verma SB (2010a) A model-data intercomparison of CO_2 exchange across North America: results from the North American Carbon Program site synthesis, *Journal of Geophysical Research* **115**, G00H05, doi: 10.1029/2009JG001229.

Schwalm CR, Williams CA, Schaefer K, Arneth A, Bonal D, Richardson AD (2010b) Assimilation exceeds respiration sensitivity to drought: a FLUXNET synthesis. *Global Change Biol*, **16**, 657–670. doi:10.1111/j.1365-2486.2009.01991.x.

Sellers P, Randall D, Collatz G, Berry J, Field C, Dazlich D, Bounoua L (1996a) A revised land surface parameterization (SiB2) for atmospheric GCMs. part I: model formulation. *Journal of Climate*, **9**, 676–705.

Sellers PJ, Tucker CJ, Collatz GJ, Los SO, Justice CO, Dazlich DA, Randall DA (1996b) A revised land surface parameterization (SiB2) for atmospheric GCMs. part II: the generation of global fields of terrestrial biophysical parameters from satellite data. *Journal of Climate*, **9**, 706–737.

Sitch S, Huntingford C, Gedney N, Levy P, Lomas M, Piao S, Friedlingstein P (2008) Evaluation of the terrestrial carbon cycle, future plant geography and climate-carbon cycle feedbacks using five dynamic global vegetation models (DGVMs). *Global Change Biology*, **14**, 2015–2039.

Song Y, Jain A, McIsaac G (2013) Implementation of dynamic crop growth processes into a land surface model: evaluation of energy, water and carbon fluxes under corn and soybean rotation. *Biogeosciences Discussions*, **10**, 9897–9945.

Still CJ, Berry JA, Collatz GJ, DeFries RS (2003) Global distribution of C_3 and C_4 vegetation: carbon cycle implications. *Global Biogeochemical Cycles*, **17**, 1006–1020.

Stöckli R, Lawrence D, Niu G, Oleson K, Thornton P, Yang Z, Running S (2008) Use of FLUXNET in the community land model development. *Journal of Geophysical Research: Biogeosciences (2005–2012)*, **113**, G01025, doi: 10.1029/2007JG000562.

Sulman BN, Desai AR, Cook BD, Saliendra N, Mackay DS (2009) Contrasting carbon dioxide fluxes between a drying shrub wetland in Northern Wisconsin, USA, and nearby forests. *Biogeosciences*, **6**, 1115–1126.

Suyker AE, Verma SB, Burba GG (2003) Interannual variability in net CO_2 exchange of a native tallgrass prairie. *Global Change Biology*, **9**, 255–265.

Vickers D, Thomas C, Pettijohn C, Martin J, Law BE (2009) Influence of disturbance and water stress on sequestration of atmospheric carbon dioxide by ponderosa pine forests. *Agricultural and Forest Meteorology*, **22**, 111–114.

Viovy N, Ciais P (2009) A combined dataset for ecosystem modelling, Available at: http://dods.extra.cea.fr/data/p529viov/cruncep/readme.htm. (Accessed March 2011).

Wang K, Dickinson RE (2012) A review of global terrestrial evapotranspiration: observation, modeling, climatology, and climatic variability. *Reviews of Geophysics*, **50**, RG2005, doi: 10.1029/2011RG000373.

Weedon G, Gomes S, Viterbo P, Shuttleworth W, Blyth E, Österle H, Best M (2011) Creation of the WATCH forcing data and its use to assess global and regional reference crop evaporation over land during the twentieth century. *Journal of Hydrometeorology*, **12**, 823–848.

Wei Y, Liu S, Post WM *et al.* (2013) 'The North American Carbon Program (NACP) Multi-Scale Synthesis and Terrestrial Model Intercomparison (MsTMIP) Project: environmental Driver Data,' *Journal of Geoscientific Model Development Discussion*, **6**, 5375–5422.

Williams M, Richardson A, Reichstein M, Stoy P, Peylin P, Verbeeck H, Kattge J (2009) Improving land surface models with FLUXNET data. *Biogeosciences*, **6**, 1341–1359.

Wilson K, Goldstein A, Falge E, Aubinet M, Baldocchi D, Berbigier P, Field C (2002) Energy balance closure at FLUXNET sites. *Agricultural and Forest Meteorology*, **113**, 223–243.

Yang X, Wittig V, Jain A, Post W (2009) Integration of Nitrogen Dynamics into a Global Terrestrial Ecosystem Model. *Global Biogeochem Cycles*, **23**, GB4028, doi: 10.1029/2009GB003519.

Yi C, Ricciuto D, Li R, Wolbeck J, Xu X, Nilsson M, Arain MA (2010) Climate control of terrestrial carbon exchange across biomes and continents. *Environmental Research Letters*, **5**, 034007.

Zeng X, Decker M (2009) Improving the numerical solution of soil moisture-based Richards equation for land models with a deep or shallow water table. *J Hydrometeor*, **10**, 308–319.

Zha T, Barr AG, Black T, Mccaughey JH, Bhatti J, Hawthorne I, Shashkov A (2009) Carbon sequestration in boreal jack pine stands following harvesting. *Global Change Biology*, **15**, 1475–1487.

Zhao M, Running SW (2010) Drought-induced reduction in global terrestrial net primary production from 2000 through 2009. *Science*, **329**, 940–943.

Zhao M, Running SW, Nemani RR (2006) Sensitivity of moderate resolution imaging spectroradiometer (MODIS) terrestrial primary production to the accuracy of meteorological reanalyses. *Journal of Geophysical Research: Biogeosciences (2005–2012)*, **111**, G01002.

Supporting Information

Additional Supporting Information may be found in the online version of this article:

Data S1. GPP SOM.pdf contains.
Data S2. Meteorology from global/reanalysis datasets.
Table S1. Mean annual GPP biases (ΔGPP) in the *ISAM-CRUNCEP* and the *ISAM-NCEP* simulations at each site. ΔCRUNCEP = *ISAM-CRUNCEP – ISAM-FLUXNET*; ΔNCEP = *ISAM-NCEP – ISAMFLUXNET*.
Figure S1. Geographical distribution of FLUXNET sites used in this study.
Figure S2. Relative differences in mean annual meteorology variables between two global reanalyses datasets used in this study.
Figure S3. Spin-up of deep soil temperature (TSoil50 m) at each site vs. years of spin-up at each site. The initial soil temperature is 1°C (i.e., 274.15 K).
Figure S4. Analysis for tree PFTs (Trop.BET, Trop.BDT, Temp.BDT, NET): (a) Daily GPP vs. daily meteorology for *Tavg*, *Srad* and *Q*. The R2 for each regression fit (line denoted as: All) were calculated using data from all the simulations. (b) Annual GPP vs. annual total *Precip* for different simulations, along with the respective *R*2.
Figure S5. Analysis for individual Trop.BET and Trop.BDT sites: Daily climatology of GPP and corresponding *Tavg*, *Srad* and *Q*. Each row of subplots corresponds to an individual site (site name on left corner). Each column shows a respective variable (GPP, *Tavg*, *Srad*, *Q*). For each subplot, the *x*-axis is the 'day of year,' and the *y*-axis is the respective variable.
Figure S6. Analysis for individual nontree C3 sites: Daily climatology of biases (Δ) in reanalyses-driven climatology of GPP, *Tavg*, *Srad*, and *Q*. Each row of subplots corresponds to an individual site (site name on left corner). Each column shows a respective variable (ΔGPP, Δ*Tavg*, Δ*Srad*, Δ*Q*). For each subplot, the *x*-axis is the 'day of year,' and the *y*-axis is the respective variable. All the biases (Δ) were calculated with respect to the *ISAM-FLUXNET* counterpart.
Figure S7. Map of C_4 fraction in herbaceous plant functional types, for (a) savanna, grass, and pasture, and (b) crop.
Figure S8. Map of vegetated land area mask used for the comparison of GPP estimates. For consistency, nonvegetated (i.e., barren land, desert, glacier, water body) grid cells were removed from all the GPP estimates (ISAM, FLUXNET-MTE, MODIS) during the construction of respective zonal means.
Figure S9. Partitioning of site-level GPP biases into sunlit and shaded components.